DOKUZ EYLÜL UNIVERSITY

GRADUATE SCHOOL OF NATURAL AND APPLIED SCIENCES

SYNTHESIS, CHARACTERIZATION OF ZnO NANOSTRUCTURES AND INVESTIGATION OF APPLICATION AREAS

by

Ahmet Emrecan ÖKSÜZ

July, 2021

İZMİR

SYNTHESIS, CHARACTERIZATION OF ZnO NANOSTRUCTURES AND INVESTIGATION OF APPLICATION AREAS

A Thesis Submitted to the

Graduate School of Natural and Applied Sciences of Dokuz Eylül University

In Partial Fulfillment of the Requirements for the Degree of Master of Science in

Nanoscience and Nanoengineering

by

Ahmet Emrecan ÖKSÜZ

July, 2021

İZMİR

M.Sc THESIS EXAMINATION RESULT FORM

We have read the thesis entitled **"SYNTHESIS, CHARACTERIZATION OF ZnO NANOSTRUCTURES AND INVESTIGATION OF APPLICATION AREAS"** completed by **AHMET EMRECAN ÖKSÜZ** under supervision of **ASSOC. PROF. DR. METİN YURDDAŞKAL** and we certify that in our opinion it is fully adequate, in scope and in quality, as a thesis for the degree of Master of Science.

Assoc. Prof. Dr. Metin YURDDAŞKAL

Supervisor

Assoc. Prof. Dr. Tuncay DİKİCİ

(Jury Member)

Assoc. Prof. Dr. Simge İRİZALP

(Jury Member)

Prof.Dr. Özgür ÖZÇELİK

Director

Graduate School of Natural and Applied Sciences

ACKNOWLEDGEMENTS

In my difficult but also pleasant process to get Master degree, there are so many people who help me to acquire Master degree. I would like to thank all of them.

Foremost, I would like to express my gratitude to my thesis advisor Assoc. Prof. Dr. Metin YURDDAŞKAL for his important recommendations, contributions. His accessibility at all times, help me a lot to finish my thesis.

I would also like to thank deeply Assoc. Prof. Dr. Tuncay DİKİCİ for constant guidance and consideration. He answered every question which I asked at any time.

I would also express my appreciation to all the administrative and academic staff in Center for Fabrication and Application of Electronic Materials for their assist and inducement. I would like to thank my dear graduate friend, Uğur KARTAL, who support and guide me during my thesis work.

Finally, I would like to express deeply my gratitude to my family. My mother Cemile ÖKSÜZ is worthy of special thanks for support and providing me comfortable environment.

Ahmet Emrecan ÖKSÜZ

SYNTHESIS, CHARACTERIZATION OF ZnO NANOSTRUCTURES AND INVESTIGATION OF APPLICATION AREAS

ABSTRACT

It is common knowledge that zinc oxide (ZnO) as a substantial semiconductor material because of its broad band gap (3.37eV) and good seperation energy (60 meV). Anodic oxidation of ZnO molecules have drawn interest because of their cost-effective synthesis, high efficiency and simplicity of the process. Anodization parameters (voltage, time, ph, electrolyte) can influence the morphology of ZnO. Also, ZnO is widely used in several implementations such as photovoltaic cell, chemical sensor, antibacterial agent and photocatalysts. Structures and different morphologies of ZnO can exert influence on its photocatalytic activity.

In this thesis, ZnO nanostructures were produced succesfully through anodic oxidation method. Before anodization, a large portion of bulk Zn was cut off into nine pieces with dimensions 3x3 cm^2. These samples were sanded up to acquire the appropriate material surface. After that, samples sonicated in ethanol, acetone and deionized water in an ultrasonic bath for ten minutes separately. Produced ZnO samples were heat treated at 300 °C for one hour with the heating rate of 5 °C/minute. The synthesized ZnO nanostructures were characterized to investigate their structure, elemental composition, photocatalytic activity and morphology with aid of X-ray diffraction, X-ray photoelectron spectroscopy, scanning electron microscopy and UV-Vis spectrophotometer. Concludes from this produced ZnO specimens can make use of as photocatalyst.

Keywords: ZnO, nanostructures, photocatalysis, anodization, semiconductors

ZNO NANOYAPILARIN ÜRETİLMESİ, KARAKTERİZASYONU VE UYGULAMA ALANLARININ ARAŞTIRILMASI

ÖZ

Geniş bant aralığı (3.37eV) ve büyük eksiton bağlama enerjisi (60 meV) sebebiyle çinko oksidin (ZnO) önemli bir yarı iletken malzeme olduğu herkesçe bilinmektedir. ZnO'nun anodik oksidasyonu, uygun maliyetli sentezi, yüksek verimliliği ve işlemin basitliği gibi sebeplerden dolayı ilgi çekmiştir. Anodizasyon parametreleri (voltaj, zaman, ph, elektrolit) ZnO'nun morfolojisini etkileyebilir. Ayrıca ZnO, güneş pilleri, gaz sensörleri, antibakteriyel ajan ve fotokatalizörler gibi çeşitli uygulamalarda yaygın olarak kullanılmaktadır. ZnO'nun yapısı ve morfolojisi, fotokatalitik aktivitesini etkileyebilir.

Bu tezde, ZnO nanoyapıları anodik oksidasyon yöntemiyle başarı bir şekilde üretilmiştir. Anodizasyondan önce, Zn kütlesinin büyük bir kısmı 3x3 cm^2 boyutlarında dokuz parçaya kesilmiştir. Bu numuneler, uygun malzeme yüzeyi elde etmek için zımparalanmıştır. Daha sonra, numunelere etanol, aseton ve deiyonize su içinde ultrasonik bir banyoda on dakika boyunca ayrı ayrı sonikasyon işlemi yapılmştır. Üretilen ZnO numuneleri 300 ° C'de bir saat 5 ° C / dakika ısıtma hızında ısıl işleme tabi tutulmuştur. Sentezlenen ZnO nanoyapıları, X-ışını kırınımı, X-ışını fotoelektron spektroskopisi, taramalı elektron mikroskobu ve UV-Vis spektrofotometre yardımıyla yapılarını, elementel kompozisyonlarını, fotokatalitik aktivitelerini ve morfolojilerini araştırmak için karakterize edilmiştir. Üretilen ZnO numunelerinin fotokatalizör olarak kullanılabileceği sonucuna varılmıştır.

Anahtar kelimeler: ZnO, nanoyapılar, fotokataliz, anotlama, yarı iletkenler

CONTENTS

Page

LIST OF FIGURES

Page

LIST OF TABLES

Page

CHAPTER ONE
INTRODUCTION AND MOTIVATION

1.1 General

Derived from a Greek word meaning dwarf, nano is a unit prefix and shows the billionth (10^{-9}) parts. However, in general, nanotechnology is the business of indirectly reducing matter to atomic size, namely nano, 10^{-9}. Nanotechnology has a important role in our future. Because molecual structure,physical characteristic and also other properties change when materials become nano-sized. Nanoelectronics and computer technology, aviation and space studies, medicine and health and textile industry are main application areas for nanotechnology.

Zinc oxide is a n-type semiconducting material. ZnO molecules have a bandgap of 3.37 eV at standard ambient temperature as 25 °C. It has also higher electron mobility than titanium oxide.ZnO has high piezoelectric tensor among semiconductors.It is relatively soft material (Özgür et al., 2005). Due to these properties, ZnO has lots of applications. Some of these are; rubber,ceramic, pharmaceutical and electronic industry, medical applications and many others (Hernández Battez et al., 2008). Great interest in ZnO nanoparticles by biological sciences such as an antibacterial, antifungal, and antifouling agent. The safeness of ZnO molecules and their compatible nature with human body made they an appropriate materials for biological applications. ZnO nanoparticles have diameters less than 100 nanometers. Process of synthesis determine the morphology of ZnO nanostructures. They may be nanorods, nanoplates, nanospheres, hexagonal, nanowires, nanotubes, nanoringsinanocages and nanoflowers. Nanoparticles have high proportion of surface area to volume. ZnO nanoparticles can be produced by different approach. These are; physical vapor deposition,ion sputtering, solvothermal method, hydrothermal methods, sol-gel methods and etc. However these are expensive and time-consuming methods. In this content, we use electrochemical anodization method. Because electrochemical methods are effective, cheaper and large scale production with desired morphology.

The photocatalytic activity of ZnO structures were analyzed by using the methlene blue (MB) degradation as common dyes under UV-Vis light illumination.

Nowadays, ZnO nanoparticles have been studied for different application areas. Ab Mateen Tantray and M. A. Shah (2020) grew ZnO nanostructures by electrochemical anodic oxidation process at 25 ºC. It is found that ZnO nanoflowers have better photo electrochemical performance than ZnO nanowires. The larger oxygen cavity on the outer layer of ZnO and lots of mobile edge sites in 2D flakes clarified the enhanced photo electrochemical performance of flower-like nanostructures. Intercalarily, photoelectrochemical performance of the ZnO nanoflowers were investigated utilizing electrochemical analyzer and it displayed a current density of ~ 60 μA cm^{-2}. This demonstrated capability of flower-like ZnO nanostructure to perform as UV-visible photoelectrode products.

Yavaş et al., (2020) produced ZnO nanoflowers by electrochemical anodic oxidation. Scanning electron misroscope figures demonstrated that duration of anodic oxidation expanded the fraction of anodized layer. Furthermore, the aspect ratio of the micrometer long nanoflower spines is increasing with the anodization time. Also, by incrementing the duration of anodic oxidation from 0 to 600 seconds, contanct angle lessens bit by bit. In conclusion, electrochemical anodic oxidation process which allows swift formation of nano-scale metal oxides can be a encouraging approach to evolve structures with tunable wettability.

Dong et al., (2016) grew a new type self-assembled ZnO nanostructure through electrochemical anodization in sodium hydroxide aqueous electrolyte. Under appropriate anodized environment, well defined nanorods were produced. The relationships between nanostructure morphology and anodization parameters were investigated using field-emission scanning electron microscopy (FESEM), X-ray powder diffraction (XRD) and energy-dispersive X-ray spectrometry (EDS). It is found that, the major variable effecting the nanostructure is performed potential,

although duration of anodic oxidation and concentration of electrolyte have important effect.

1.2 Organization of the Thesis

The primary objective of this thesis is to produce nano-scale ZnO samples through anodic oxidation method. Considering experiences from previous work, anodization parameters were determined as mentioned in Table 3.1. Another major point of this work is to develop photocatalytic activity of ZnO samples to reduce the contamination of synthetic dyes. This study proved that decrement of contamination in synthetic dyes can be achieved with ZnO nanostructures.

X-Ray Diffraction (XRD) measurement was implemented to observe crystal structure of ZnO samples. Scanning electron microscopy (SEM) assisted to survey surface morphology. Elemental survey of ZnO samples were performed with the help of X-ray photoelectron spectroscopy (XPS). The reduction of absorbance intensity of the methylene blue(MB) dye was observed utilizing the UV-Vis spectrophotometer.

In Chapter 2, theoretical background of ZnO, their synthesis methods and their applications were discussed. Additionally, general principles of anodization method were explained in detail. In Chapter 3, experimental methods of anodic oxidation technique were described. Also, characterization techniques were stated exhaustively. In Chapter 4, results of these experiment were showed and explained scientifically. Overall conclusion of this thesis and future plans are given in Chapter 5.

CHAPTER TWO
THEORETICAL BACKGROUND

2.1 Semiconductor Materials

In the main, the chemical composition and the crystallographic structure, the existence of different defects and impurities (both intentional and unintentional), and the dimensions of the semiconductor are correlated to the primary factors that identify fundamental properties of semiconductors. The chemical composition and the crystallographic structure define the electronic band structure which has the great impact on the semiconductor features (Yacobi, 2005). Semiconductors are divided into intrinsic and extrinsic semiconductors.

The instrinsic semiconductors has no impurities or defect. In these,the characteristic of the crystal are identified by the features of atoms of the semiconductor material. In semiconductors, several impurities are intentionally insterted to fabricate materials and devices with wanted features. At that rate, the material is mentioned to as extrinsic, and the operation of placing impurities into the lattice is called doping (Sharma, 2001). Based on the impurity atoms,the extrinsic semiconductors are called n-type and p-type semiconductors.

The operation of placing impurities into the lattice is named doping. The endavor of free carriers by dopants needs them being ionized. The ionization of the dopants is based on the heat energy and the location of the contamination degree in the band gap of a semiconductor. Contaminations that promote electrons to the conduction band are named donors, and these that provide holes to the valence band are acceptors (Yacobi, 2005).

An electron donor dopant integrated in the crystalline, liberates a movable conduction electron within the crystal structure An extrinsic semiconducting material

that integrated with electron donor atoms is named an n-type semiconducting material, inasmuch as the preponderance of charge carriers in the crystalline are negative electrons. An electron acceptor dopant composing a space that an electron ought to be named a hole that is capable to pass through the crystalline similar to a positively charged molecule, is an atom which admits an electron from the lattice. When the generality of charge carriers in the crystalline are positive holes, an extrinsic semiconductor is termed p-type semiconductor which has been doped with electron acceptor (Neamen, 2003). The crystal structure and energy band diagram of n-type and p-type semiconductor is demonstrated in figure 2.1 and figure 2.2.

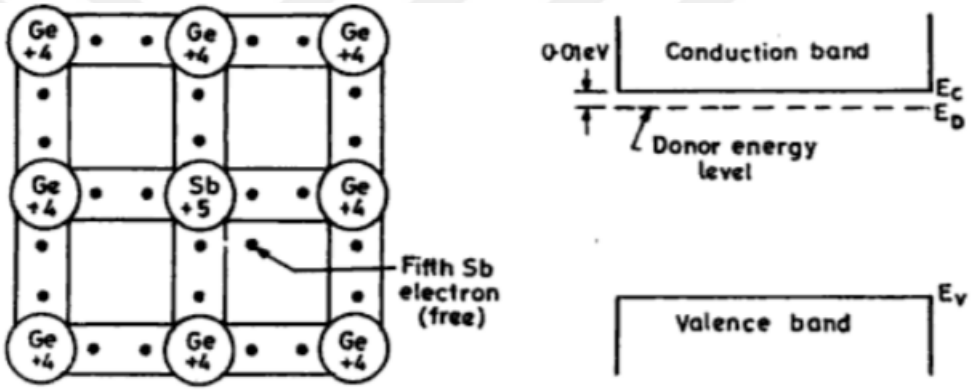

Figure 2.1 Crystal structure of n-type semiconductor and energy band diagram (Sharma, 2001)

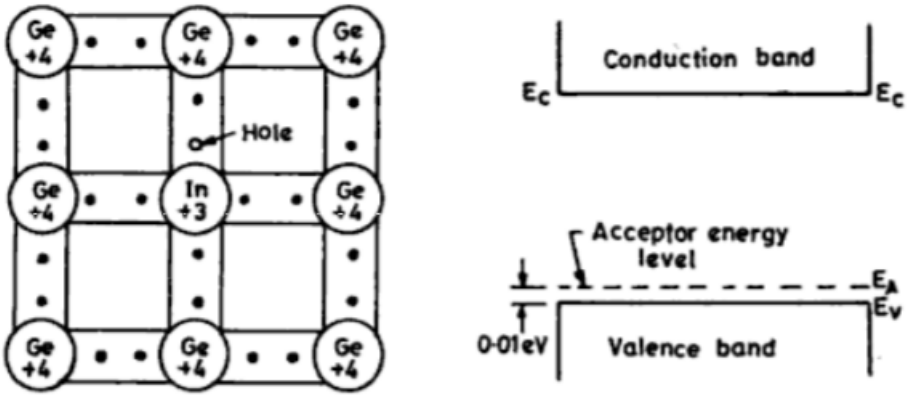

Figure 2.2 Crystal structure of p-type semiconductor and energy band diagram (Sharma, 2001)

2.1.1 General Brief of Zinc Oxide

Zinc oxide is an inorganic molecule and insoluble in water. It has many usage areas such as cosmetics, food supplements, plastics and seramics. Even though it is obtainable in natural state, the processing of zinc oxide generally must occur for manufacturing applications. In natural state it is called mineral zincite which generally include manganese and various impure chemical substances (Klingshirn, 2007). ZnO is a broad-band gap material in II-VI semiconductor category. The doping of the semiconductor because of oxygen gaps or zinc interstitials is n-type. Zinc oxide has a great thermal capacity and good thermal resistance.

Although zinc oxide is dissoluble in H_2O, it can dissolve in acids and bases. zinc oxide melt at 1975 celsius degrees which is very high point. ZnO performs reaction slowly with oils which contain fatty acids to fabricate the coincident carboxylates. ZnO composes cement-like materials when combined with a powerful hydrous solution of $ZnCl_2$ (zinc chloride) and these are expressed as zinc chloride hydroxide monohydrate. This cement uses in dentistry (Nicholson & Parker, 1998).

Hexagonal wurtzite and cubic zincblende are two primary shape of crystallization of zinc oxide. These crystal structures are shown in figure 2.3. The wurtzite structure is mosre stable at environmental circumstances (Niederberger, 2007). Stabilization of zincblende structure of ZnO can enhance by forming ZnO on substrates with cubic lattice form. In either situations, the zinc and oxide centers are tetrahedral, the most distinctive geometry for Zn(II). ZnO transform to the rocksalt theme at comparatively intense pressures nearly 10 Gpa (Özgür et al., 2005).

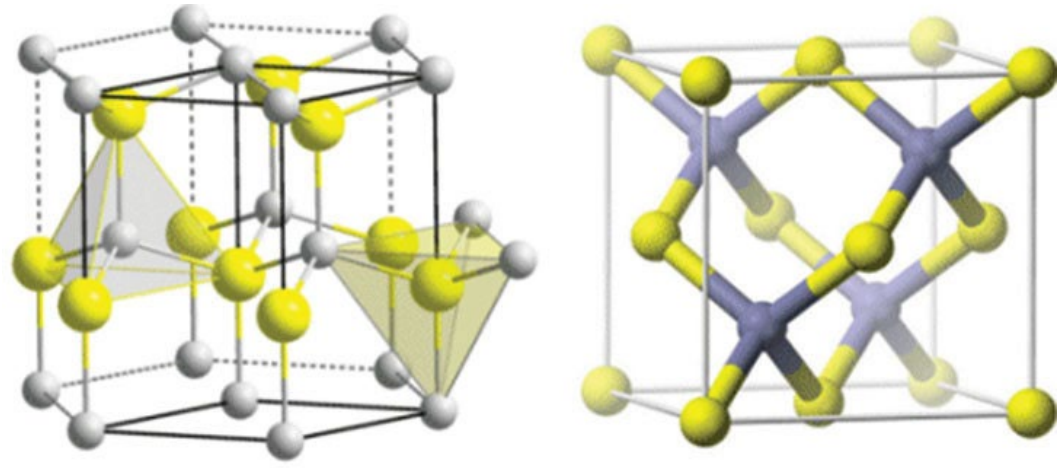

a)Wurtzite structure b)Zinc blende structure

Figure 2.3 Crystal structures of ZnO (France et al., 2016)

ZnO is in some degree soft material with imprecise hardness of 4.5 on the Mohs scale. Its elastic constants are lower than those of proper III-V semiconductors, like GaN. ZnO with large thermal capacity and thermal conductivity and high melting point is advantageous in ceramics (Porter, 1991). Between the tetrahedrally bonded semiconducting materials, ZnO has the greatest piezoelectric tensor (Dal Corso, Posternak, Resta, & Baldereschi, 1994). Therefore it is technologically major material, which needs a large electromenhanical coupling for piezoelectrical applications.

The majority of ZnO molecules are *n*-type semiconductors, even in the nonexistence of intentional doping. Nonstoichiometry is generally the provenance of n-type character, but the matter is still under discussion (Look, Hemsky, & Sizelove, 1999). An another approach has been suggested, on the basis of theoretical computations, that unintended substitutional hydrogen impurities are liable. Manageable n-type doping is simply obtained by switching Zn with group-III elements such as Al, Ga, CL_2 or I_2 (Kato, Sano, Miyamoto, & Yao, 2002).

2.1.2 Industrial Synthesis of Zinc Oxide

In the indirect method also named French process, metallic zinc is dissolved in a graphite melting pot and evaporate at temperatures over 900 °C . To achieve ZnO, zinc steam intreact with the oxygen in the atmosphere keep company by a decrease in its temperature and bright luminescence (Porter, 1991).

The direct method also named American process begin with various polluted zinc composites, like zinc ores. To obtain zinc vapor,the zinc precursors are reduced by heating with a basis of carbon source. Then zinc vapor oxidized as in the indirect process. The quality of final product is worse than indirect one (Klingshirn, 2007).

A minor number of industrial manufacture contain wet chemical process, which begin hydrous solutions of zinc salts, from which $Zn(OH)_2$ zinc hydroxide is precipitated. The solid sediment is calcined at temperatures about 800 °C.

2.2 Synthesis Methods of Zinc Oxide

The diversity of nanosctrures of ZnO expresses that nano-scale ZnO can be categorized between novel substance with prospect applications in numerous domain of nanotechnology. Also ZnO can consist of in one dimensional, two dimensional and three-dimensional formations.

ZnO molecules present a large scope of features. There are various of techniques for generation of ZnO. Vapor deposition, electrochemical anodization, sol-gel approach and solvo- hydrothermal approach are the general synthesis methods which allows achieving output with particles differing in form, dimension and space structure (Kolodziejczak-Radzimska & Jesionowski, 2014a).

2.2.1 Physical Vapor Deposition

Physical vapor deposition alludes to a diversity of vacuum evaporation strategies. Major operations for example sputtering and deposition are utilized in PVD to produce a steam, within the shape of particles such as anion, cation or molecule of the coating substance provided from a target source. These particles are at that point carried to and stored on the substrate surface, coming about in coating arrangement. The melting temperature of the target material is considerably higher than the substrate temperature in PVD procedures, it can achieve to coat temperature sensitive materials (Li & Aik Khor, 2019).

The diagrammatic representation of PVD system is illustrated in figure 2.4. The technique includes four stage. Firstly, evaporation of the material to be deposited by a great deal of energy origin like an ion beam or electron beam. Secondly, movement of the vapor to the substrate to be coated. Thirdly, response among the metal elements and suitable reactive gas in the time of the transport stage. Finally, deposition of the coating at the substrate surface (Makhlouf, 2011). PVD innovation contains a wide extent of deposition methods and also procedures incorporate method on the basis of sputtering, whether by laser beam or by ion beam. PVD is additionally utilized to portray the evaporation from arc origin with filter or non-filter. Generally, this strategy separated into bunches as evaporation and sputtering. Both strategies have been assisted created into a few particular strategies (Faraji, Kim, & Kashi, 2018).

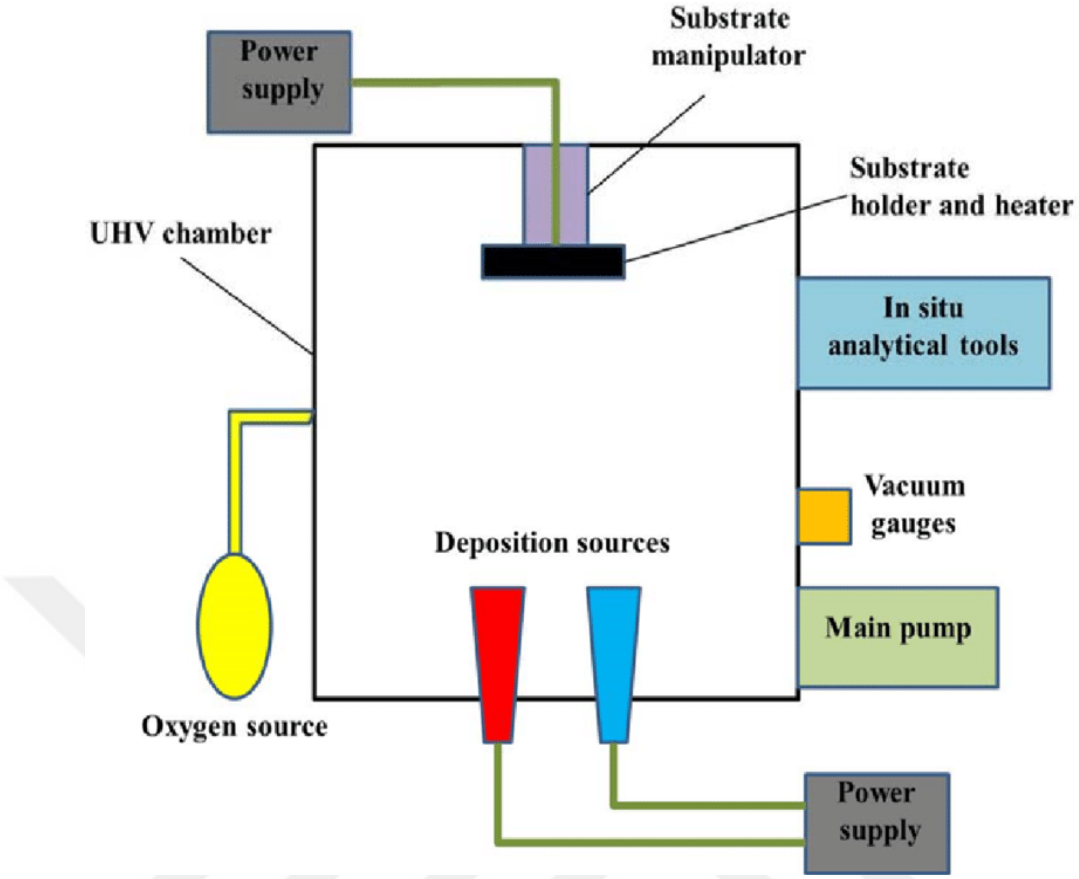

Figure 2.4 Diagrammatic representation of a fundemental PVD system (Y. Wang, Chen, Wang, & Zheng, 2014)

2.2.2 Chemical Vapor Deposition

Chemical vapor deposition, one of the notable production strategy, utilized in the wide scope of facilities for intense heat assurance, erosion preservation, and blends of both. At this point, via chemical process from gaseous -state or steam-state precursor the film is precipitated on the surface of the base material. This process requires an excitation energy. Various gaseous are passed into the vacuum chamber from inside of entrance. The separation among the species are occurred (Madhuri, 2020). In this way, the recently composed particles are deposited on the warmed up base material as seen in Fig 2.5.

The key distinctive feature of CVD is that the deposition of material onto the substrate is a multidirectional sort of deposition, though PVD is a line-of-site impingement sort of deposition. Microproduction operations broadly utilize CVD to deposit materials in different shapes, containing monocrystalline, polycrystalline, amorphous, and epitaxial (Behera, Mallick, & Mohapatra, 2020).

In comparison with different synthesis method, CVD has the most elevated level of control for the generation of 2D nanomaterials. The CVD method supplies enormous generation of 2D nanomaterials with superior crystal quality, purity, and restricted imperfection on the substrates. The 2D nanomaterial arranged by the CVD method is utilized in a assortment of viable applications such as hardware, optoelectronics, and sun based cell device. But within the case of CVD procedure, it is continuously requesting the exchange of nanosheets from deposited substrates for further examination. Additionally, higher generation cost is another disadvantage (Pottathara, Grohens, Kokol, Kalarikkal, & Thomas, 2019).

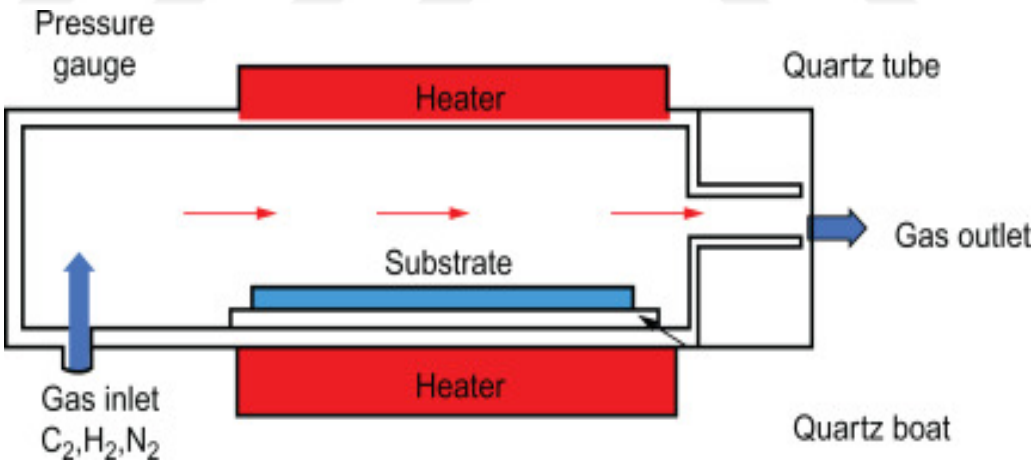

Figure 2.5 Typical set up for CVD technique (Madhuri, 2020)

2.2.3 Sol-Gel Method

Sol–gel method, as the term proposes, include a solution and consist of two main process which are gelation and deposition on a substrate. The beginning substance is a metal alkoxide reacted in an appropriate dissolvent, frequently ethanol. The substance is hydrolyzed by adding a little water thus it composes a polymeric material, assisted by setting the solution lightly acidic. The final product is a slack gel with fluid stuffed pores that can be impelemented to a substrate (Macleod, 2013).The sol-gel approach is regarded as efficient to alter the outer layer of substrates. Acquiring of a large surface field and fixed surfaces is the greatest significant superiority of the sol-gel approach. The characteristic features of the substances acquired by the sol-gel approach are linked to the circumstances of experimentation implemented (Yilmaz & Soylak, 2019).

The sol–gel technique joins the benefits of both non-organic and natural features. This strategy may be utilized in an assortment of substrate surfaces. The sol–gel method (Fig. 2.6) is moderately economical and may be executed at a lower temperature, which permits management of the product's synthetic formation. The upsides of utilizing this strategy in the clinical area is the capacity to create a thick coating to forestall process of corroding, a connection among the substrate and sol–gel coating to develop attachment, may be utilized on any geometrical form, and may generate materials without any contamination successfully (Makhlouf & Rodriguez, 2019).

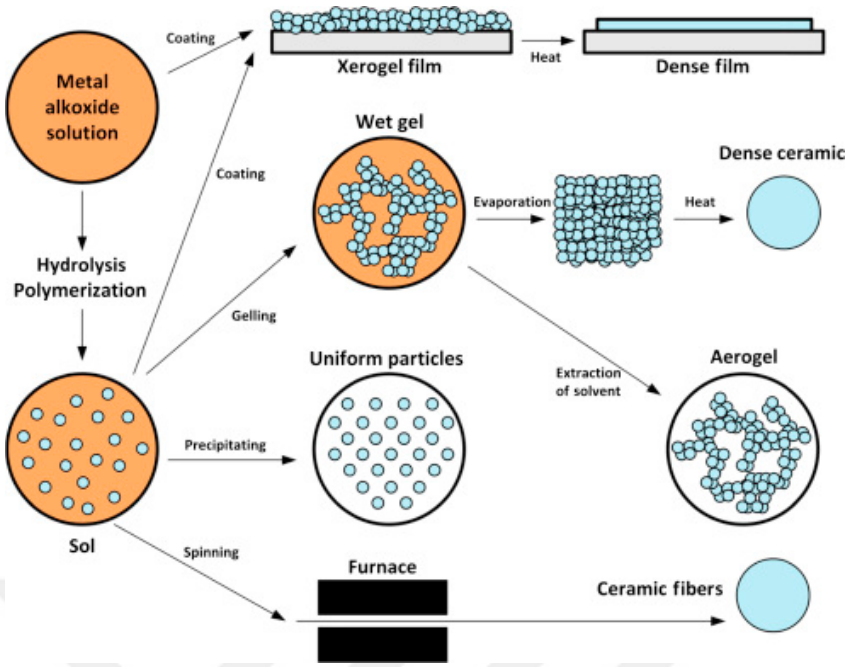

Figure 2.6 Schematic diagram of sol-gel process (Makhlouf & Rodriguez, 2019)

2.2.4 Hyhdrothermal Method

Hydrothermal technique may be characterized as a strategy for blend of monocrystalline that relies upon the dissolvability of inorganic solid in very warm water in case of intense compression. Development of monocrystalline is acted in a mechanism comprising a metal pot named an autoclave which is illustrated Figure 2.7. A temperature gradient is kept up among the contrary edges of the development cell. At the warmer finish the nutrient solute breaks up, whilst at the cooler finish it is deposited on a seed crystalline, developing the wanted crystalline (Kafle, 2020).

In hydrothermal synthesis, the chemical impurity of the powder materials is lower because of beginning with great purity precursors. In the time of crystallization methodology, developing crystallites are prone to refuse contamination appearing in the growth atmosphere. As a result, it is normal that contamination such as ions come from metal salts or pH fixing agents cleared from the mechanism in partnership with the crystallization solution. Nonetheless, a few instances may be adsorbed to outer layer of the molecules because of the colloidal collaborations among the particles and present ions (Suvaci & Özel, 2020).

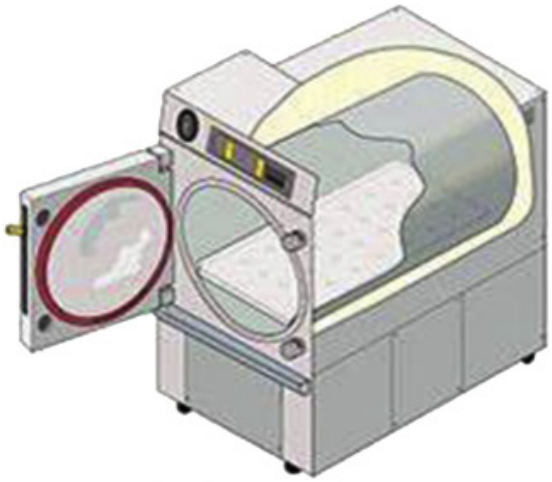

Figure 2.7 Cutaway illustration of a cylindrical-chamber autoclave (Kafle, 2020)

2.2.5 Solvothermal Synthesis

Process of solvothermal production is valuable for the generation of magnetic materials with developed physical and chemical features operable to both mechanical and medical territories. In the solvothermal production approach, hydrous or non-hyrous dissolvents may be utilized to produce magnetic materials with exact domination on the grain extent, form, and crystal phases. These physical properties may be modified by replacing specific investigational variables, for example the duration and temperature of the reaction, dissolvent, surfactant, and starting substances (Shaikh, Ubaidullah, Mane, & Al-Enizi, 2020).

The operation includes the blending of the precursors in the solvent and afterward sealing them in an autoclave. The autoclave is heated at temperatures over the boiling degree of the solvent. The autoclave acts as a unopen network that raises the temperature and pressure of the solution and afterwards crystallizes the dissolved substance. With appropriate choice of the precursor structure and the reaction circumstances, it is feasible to accomplish very low contamination and homogeneously distributed nanoparticles with a very limited size distribution. This process needs no high-temperature operations. In spite of being a low-temperature production, this

process offers phosphors with great crystallinity. The dimension, morphology, and phase structure of the phosphors signifimaytly are based on the reaction temperatures, pH, solvent, and the precursor formations. An important drawback of this process lies in its powerlessness to generate huge amount of phosphors in a one go. The tiny-scale autoclaves restrict the large-scale generation of phosphors (Nair & Dhoble, 2021).

2.2.6 Green Synthesis

Approach of green synthesis is an arising territory in the area of biotechnology and gives financial and ecological advantages as an option to other synthesis process. At this technique, nontoxic secure reactive agents which are environmentally suitable and biologically safely are utilized. Different organic assets accessible in the living world such as herbal extracts, cyclodextrin, chitosan and lots of have been investigated for the production of nanostructures based on metal oxides. The usage of herbal extract in the green synthesis of nano-scale based metal oxides has brought a significant consideration as a direct methodology (Mtibe, Mokhothu, John, Mokhena, & Mochane, 2018).

Liang et al. (2011) studied on the function of peptide molecules in morphology confirmation of ZnO nanostructures. The researchers discovered that the structure of ZnO crystalline is based on the interactivity of peptide molecules with plane of ZnO surfaces. The adsorption mechanism of peptide molecules on ZnO taking after the adsorption development hindrance instrument and peptide series affected the adsorption instrument, which influenced morphology of ZnO crystalline (Chhipa, 2019). Green synthesis of ZnO via plants, microbes, and other routes are illustrated in figure 2.15.

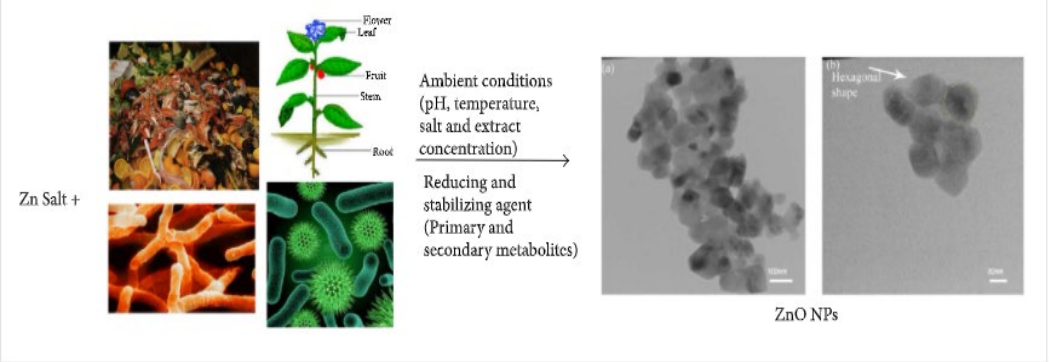

Figure 2.8 Green synthesis of ZnO via plants, microbes, and other routes (Naveed Ul Haq et al., 2017)

2.2.7 Arc Discharge Method

In arc discharge approach, two very low impurity graphite electrodes as positive electrode and negative electrode are kept at small distance separated in a helium environment. In these conditions, a portion of the carbon evaporated from the positive electrode, liquefied as a rigid cylindrical deposit on the negative part of the bar. The important case within the arc–vaporization process is the current exerted. Greater current implementation can bring about a rigid, sintered substance with small number of liberated nanostructures. Hence, the current might be hold at the lowest feasible. Utilizing arc-discharge technique, separate carbon nanotubes can be accomplished in normally some hundred microns length (Raval, Joshi, & Chejara, 2018).

Multi-walled carbon nanotubes (MWCNTs) are generated by arc discharge in the absence of any accelerator, whereas blended accelerator (Fe, Co, and Ni) are needed for the fabrication of singe-wall carbon nanotubes (SWNCTs). Generally, CNTs grown by arc discharge indicate a superior level of formational excellence; nevertheless, various factors (temperature of the cell, the formation and concentration of the accelerator, the availability of hydrogen, etc.) impact their dimension and composition. Newly, different electrodes and different chemicals have been operated for the production of CNTs utilizing arc discharge method (Ferreira et al., 2018). A greater expansion in MWNT generation ratio was anticipated by utilizing denser graphite rods in bigger and effective arc reactors. This expectancy was accomplished with the structure of a wide-ranging arc reactor with a 350-l chamber adequate for

evaporating up to nearly 70-mm-diameter graphite rods. The round negative electrode terminal deposits, acquired at this upscaled operation, include a supple core within the external rigid shell (J. Yan, Fan, & Zhi, 2012). Schematic illustration of arc discharge method is given in figure 2.9.

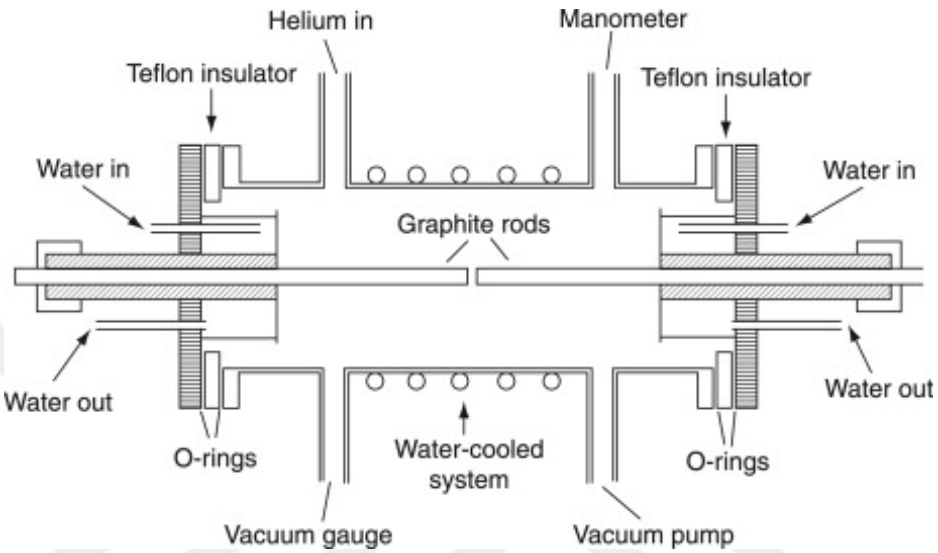

Figure 2.9 Schematic illustration of arc discharge method (J. Yan et al., 2012)

2.3 General Principles of Anodization Methods

Anodization or anodic oxidation is an admirably accepted surface adjustment method for valve metals that generate shielding layers. In the time of anodic oxidation, a consistent voltage or current is implemented between the positive electrode and negative electrode, electrolytic cell reactions (redox reactions) in blend with diffusion of ion cause to the oxidation of on the outer layer of positive electrode (anode) (Yao, Lu, & Webster, 2010). Anodic oxidation is a process related with electrochemistry operation which has been utilized to improve outer layer of implant. In this method, the zinc is set as a positive electrode in an electrolytic cell where a prearranged potential is implemented prompting the process of oxidizing of the outer layer of zinc. It comes about within the creation of an oxidized film with changeable features with respect to the processing parameters. The anodic oxidation method is based on various factors such as applied voltage, electrolytic concentration, duration of anodic oxidation

, pH and temperature of anodic oxidation. A greater clinical achievement ratio was noticed for the anodically oxidized titanium implants in comparison with polished titanium surfaces of analogous structure (Souza et al., 2018). The reaction mechanism which is showed in figure 2.10 of anodization is as follows:

$$\text{At anode: } Zn \longrightarrow Zn^{+2} + 2e^- \quad Zn^{+2} + 2OH^- \longrightarrow Zn(OH)_2 \tag{2.1}$$

$$Zn(OH)2 \longrightarrow ZnO + H_2O \tag{2.2}$$

$$\text{At cathode: } 2H^+ + 2e^- \longrightarrow H_2 \tag{2.3}$$

$$\text{Dissolution: } ZnO + HA \longrightarrow ZnA + H_2O \tag{2.4}$$

where '*A*' represents HCO_3^- ions from the bicarbonate electrolyte in dissolving procedure.

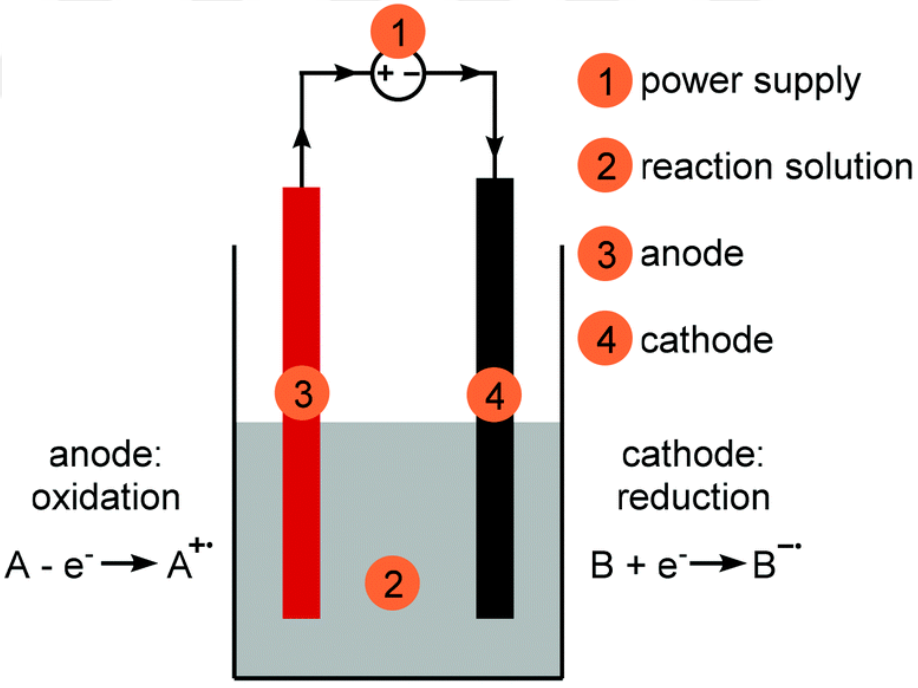

Figure 2.10 Schematic illustration of an anodization process (Schotten et al., 2020)

2.3.1 Effect of Type and Electrolytic Concentration

Mateen Tantray and Shah (2020) investigated the influence of different electrolytes and concentration of electrolyte. In the production of zinc oxide nanowires, dissimilar class of electrolytes extending from sodium hydroxide to very hydrogen fluoride hydrous solution has been reported by several scientists. Between these, bicarbonate solution appears to be the most encouraging solution as it permits the creation of nanowires with large amplitude. With the aim to analyze the influence of concentration on the outer layer of zinc and development of nanowires, a good deal of research were performed at standard as 25 °C maintaining the duration of anodic oxidation for 10 minutes and potential at 10 V while differing the concentration of solution among 50 mM and 200 mM. It was discovered that excessive concentration in partnership with intense voltage generates noteworthy fractures and flakes on positive electrode surface. The cause could be, under definite laboratory circumstances in the time of anodic oxidation, the slit called as etching of the Zn surface at positive electrode surface is controlled in base of the electrochemistry operation and on implementing the steady voltage later, the dissolution of the Zn starts that causes to the generation of micrometrical spaces on the outer layer of the metal. More profound examination of the inside surface uncovers intermittent flake like formation that develop inside the single grains, clarified by a regional super saturation brought about by generally intense concentration of Zn^{+2} in Figure 2.11b and Figure 2.11c. Furthermore, SEM investigations appeared that concentration of electrolyte may contribute to the development of nanowires to an awesome degree. Moreover, for cost of pureness of film, at less concentration of 50 mM an oxide layer formation on zinc surface is expanded underneath that nanowires are developed that were watched through SEM (Figure 2.11d) that demonstrates bicarbonate electrolyte concentration has a critical influence in fracturing and development ratio of nanowires (Mateen Tantray & Shah, 2020).

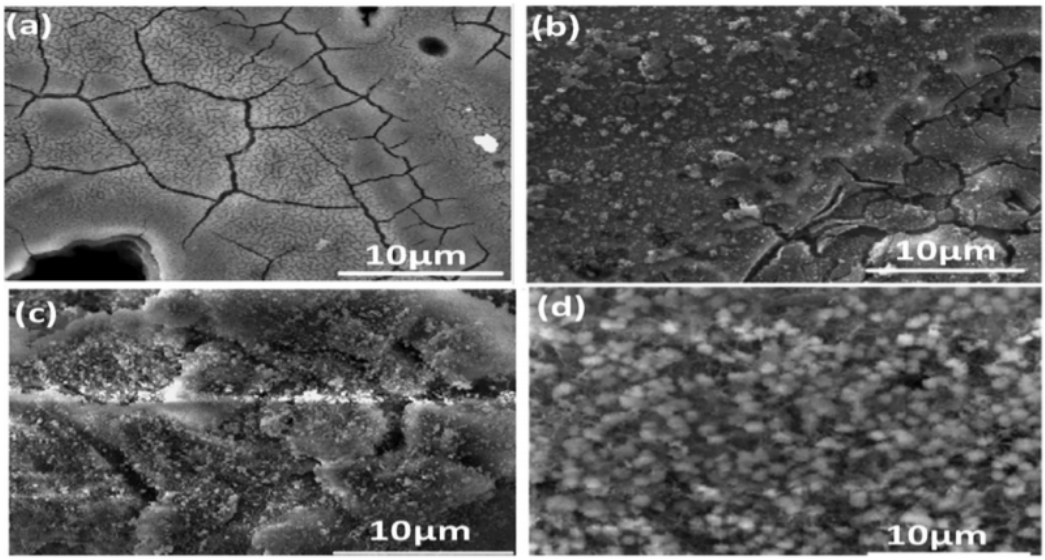

Figure 2.11 SEM displays of ZnO at various concentrations of hydrous $KHCO_3$ solution (a) 200 mM (b) 150 mM (c) 100 mM and (d) 50 mM (Mateen Tantray & Shah, 2020)

2.3.2 Effect of Applied Voltages

Dong et al. (2016) was studied the influence of implemented voltages on the morphology in 0.1 M NaOH solution for 60 minutes at various potentials between 5 V and 40 V. Nanostructures show up on outer layer of the anodized ZnO films. Notwithstanding, their transverse section morphologies under the grainy layer were dissimilar. Figures 2.12a, 2.12b and 2.12c displayed the poriferous morphology acquired with 5 V, 7 V and 9 V owning an average thickness of approximately 1.60 µm. When the implemented potential enhances to 12 V, partitioned linear cells having thickness of approximately 7-8 µm shaped as seen in Figure 2.12d. The morphology of nanoporous composition may be based on to inadequate procurement of V. In equation 2.5, E changes straight with V and conversely with oxide thickness d, that may be expressed as below:

$$E = V/d \tag{2.5}$$

Where E is the magnitude of the electric field, V is the potential difference between the plates and d is oxide thickness. As thickness of oxide layer enhances with chemical reaction advance, power of E debilitates below stable V. When V is less than 9 V, correspondent E is powerless to mobilize oxygen including ions along the oxide layers to shape ZnO and oxidation transaction will finally shut down. Consequently, the thickness of entire layers arranged beneath various potentials remains steady about 1.6 μm. Because of relocation ratio of anions lessening with increment of d, remaining OH- anions are proned to dispersed liberally and penetrate shaped ZnO irregularly, bringing about nanoporous structures. When V raises to 12 volt potential, the crucial point of electric field E and oxide layer thickness d are going to be fixed at a stable condition, bringing about unaltered oxidization and dissolving ratio. As a result, dynamic balance will be achieved, driving to generation of organized nanorod arrays (Dong et al., 2016).

As the potentials raise to intense levels of 20 V, 30 V and 40 V, ZnO layers get denser. Nanorod arrays lie at 90 degrees to the substrates with spaces or fractures among layers. Within the spaces, various nanostructures seem analogous to the granular surface. The lack of continuity of anodic layers may be caused to the rapid formation of layers and intense generation of oxygen in the course of anodization. As anodization operation is speeded up beneath intense potentials, oxygen is assumed to liberate swiftly. Powerful oxygen output can damage regional tension of oxide/substrate link. For this reason, delicate nanorods arrays are appropriate to split through parallel to the plane of the horizon, and broad distance formational system is devastated. Concerning the nano-scale particles which are sandwiched among independent layers, their generation gets from dissolving of grown nanorods via OH- etching. Moreover, further holes or breaks are available in inner side of layers with raising potentials because of greater quantity of oxygen release (Dong et al., 2016).

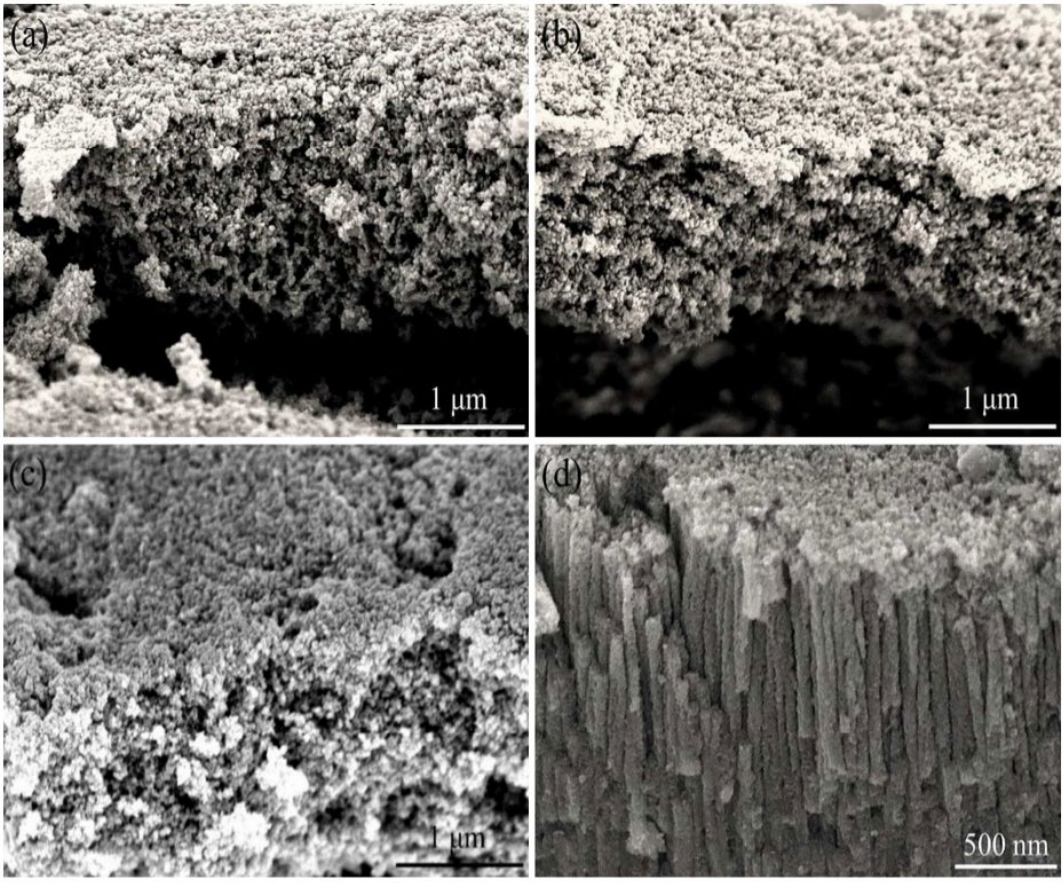

Figure 2.12 FESEM cross-section displays of anodic films produced in 0.1 M NaOH aqueous electrolytes for 1 hour at different potentials of (a) 5 V, (b) 7 V, (c) 9 V, and (d) 12 V (Dong et al., 2016)

2.3.3 Effect of Anodization Time

Figure 2.13 displays the FESEM images of the ZnO nanoflake arrays developed by anodic oxidation at standard ambient temperature as 25 °C utilizing dissimilar anodic oxidation durations. At 30 minutes, unfinished creation of small nanoflake shape was perceived, whereas 60 min and 90 min of anodic oxidation indicated a further finished creation of nanoflake arrays. The dimensions of nanoflakes widened as the duration of anodic oxida-tion raised. As compared to the nanoflake arrays shaped after 60 minutes, the ones formed after 90 minutes were more filled and uniform. This demonstrates that duration of anodic oxidation assumes a part in the identification of nanoflake dimension and dispersion. Moreover, the impact of stirring in the time of the anodic oxidation process was examined.In addition to previous anodic oxidation parameters, ZnO nanoflake arrays developed by anodic oxidation at standard ambient temperature

as 25 °C and 10 V for 90 min with light stirring in 0.0500 M $(NH_4)_2$ SO_4 and 0.0250 M NaOH solutions. It tends to be seen that with stirring, the nanoflakes that shaped were greater consistent and tinier. The reaction was quicker with stirring as a consequence of the dispensed OH^- ions interior the electrolyte. Nonetheless, the ZnO shaped is going to solvate because of stirring that avoids it from forming to bigger nanoflakes (Goh, Adnan, & Farrukh, 2011).

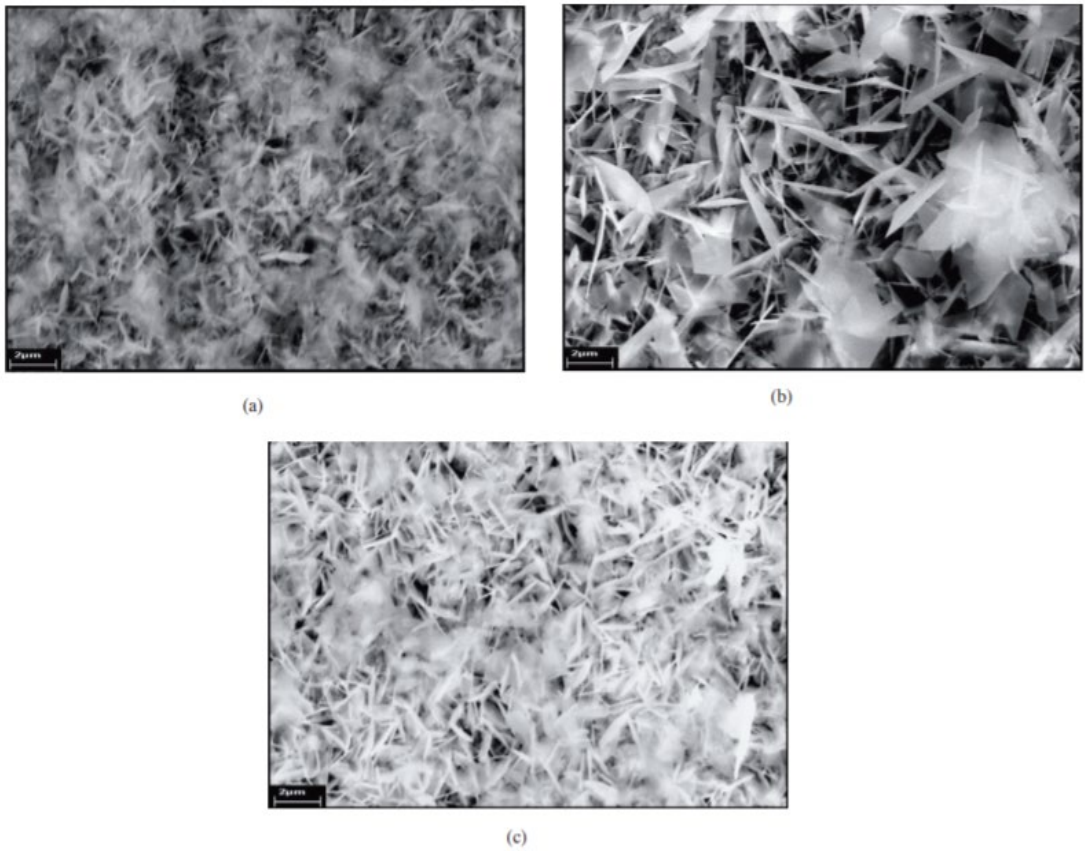

Figure 2.13 FESEM images of zinc foil anodized at 10 V in 0.0500 M $(NH_4)_2$ SO_4 and 0.0250 M NaOH electrolyte blend at ambient condition utilizing dissimilar anodic oxidation durations: a) 30 min, b) 60 min, and c) 90 min (Goh et al., 2011)

2.3.4 Effect of Temperature

Generally, the effect of temperature changes among solutions. In acidic solutions, temperature shows to have a major influence on the morphology of nanostructure just for nominal level of the anodic oxidation potential and concentration of solution. In greater potentials, concentration and duration, the effect of aforementioned variables is dominant in comparison with temperature. Films acquired with H_3PO_4 at 0 °C displayed intense morphologies in the absence of clearly defined formations. Anodic oxidation with HNO_3 at nominal potential (1 V) and nominal condition (0 °C) led to in a small increment in the portion of nanostructures per unit of area, with lower dimensions in comparison with to nanostructures which produced at 10 °C. Nevertheless, at intense potential no considerable dissimilarities were noticed. Temperature fails to have a considerable effect on nano-scale structures acquired with NaOH at 1 V, but at 40 V the decrease of temperature results in a nearly unspecific outer layer. Nominal temperature (0 °C) anodic oxidation with HCl solution led to morphologically denser formation with non-uniform nano-scale formations. Analogue morphologies were acquired at 0 °C and 10 °C with $C_2H_2O_4$. Films acquired at 0 °C with $KHCO_3$ and 1 V are consisted of denser nanowires in comparison with grown at 10 °C. In addition, at intense potential it displays which the etching operation predominates, resulting in the entire dissolution of the Zn substrate (Ramirez-Canon, Miles, Cameron, & Mattia, 2013).

2.4 Application Areas of Zinc Oxide

On account of their various features, both chemically and physically, ZnO molecules are broadly utilized in many fields. They have an influence on a considerable amount of implementations, alternating from rubber to electronics and from dyes to cultivation. Figure 2.14 displays global usage of ZnO by region.

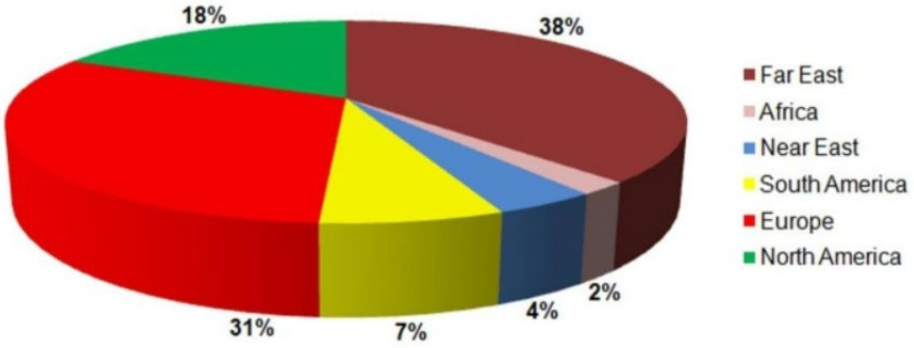

Figure 2.14 Global usage of zinc oxide (Kolodziejczak-Radzimska & Jesionowski, 2014b)

2.4.1 Photocatalysis Applicaton of ZnO

Diverse semiconducting nanomaterial have been broadly utilized to figure out energy and climate issues with their great photocatalytic features (Kudo & Miseki, 2009). Over the past few years, many scientists have concentrated on the generation of hierarchical semiconducting nanomaterial owing to their benefits, containing high surface area, porous shape, enhanced light harvesting, etc (X. Li, Yu, & Jaroniec, 2016).

ZnO has aroused a curiosity in lots of areas of photocatalysis implementation, for example the deterioration and ecological contaminants and H_2 production. Also, due to its cost-effective production, non-poisonous nature and effective photocatalytic performance it has attracted attention. Because ZnO molecules (3.37 eV) have nearly the identical band gap as TiO_2 (3.2 eV), its photo-catalytic ability is expected to be identical with TiO_2. Furthermore, ZnO molecules are moderately lower costly in comparision with TiO_2 molecules, thus the utilization of TiO_2 molecules are expensive for photocatalysis implementation. The streamlined photocatalysis decay operation of semiconducting material, for example ZnO includes 4 steps. Firstly, stimulation of ZnO through UV irradiation. The second step is generation of excitons. The third step is development of diverse reactive oxidative species (ROSs). The final step is oxidazation of the organic chemicals or reduction of the water by ROSs. H_2 production is a photoe-lectrochemical technique in that hydric oxide may be poured. Nevertheless,

the extensive band gap of ZnO can be exclusively triggered in the UV domain, that creates for lower than 5% of the entire energy of the solar spectrum. Besides, the quick reunification of photogenerated electron-hole couples in ZnO usually cause reduced photocatalytic performance. Consequently, diverse molecules, such as N and C, have been doped into ZnO to improve the solar power usage. For instance, N- and C-doped ZnO hierarchical photocatalysts have been discovered to absorb of light effectively in visible and ultraviolet domain because of their lower-level band gap energies (Xia, Wang, Chen, Zhou, & Xiang, 2016).

2.4.2 Electronic Application of ZnO

For electronic instrument, the fascination of ZnO originates from having high breakdown strength and high saturation velocity. ZnO supplies great radiation hardness compared with other prevalent semiconducting materials, such as Si, GaAs, CdS, and GaN, improving the functionality of ZnO for space industry. Optically pumped UV laser effect in ZnO has been indicated at both nominal and high temperatures but effective electrically induced lasing expects forward advancements in the empirical ability to produce good quality p-type ZnO material. During the past ten years, scientist have advanced important theoretical and experimental improvement covering the p-type dopability of ZnO, with 1017 cm-3 range hole concentrations reasonably accomplished with material stability persisting for more than a year. Eventually, ZnO semiconducting materials may be doped with transition metal ions to generate attenuate magnetic materials, which may compose a ferromagnetic state, an antiferromagnetic state and a general spin glass. The substantial subject is that the Curie temperature may be beyond standard ambient temperature as 25 °C (Litton, Reynolds, & Collins, 2011).In this type of situation form the basis for spintronic devices.

In a number of ways, ZnO molecules are regarded to bge production and great optical features. Nevertheless, replicable and stabilization of p-doping maintains to be the formidable issue to generating bipolar instrument derived from ZnO molecules. Electronically, the reasonably nominal mobility of ZnO molecules in comparison with GaN molecules and almost fourfold greater electron–phonon coupling and relatively

weak thermal conduction are significant defect on the account of ZnO molecules. Although, transparent thin film transistors (TFTs) composed of ZnO molecules seem to have future. Moreover, the potential global indium deficiency in front of expanding request for indium tin oxide (ITO) appears to be triggering the discovery of ZnO-derived materials, that if accomplished, can turn into an enormous implementation field. Optically, ZnO molecules are required to display intense p-type conduction besides great caliber heterojunctions on the account of achievement of desired light emitters. An important dominance of ZnO molecules is their intense 60-meV exciton binding energy in comparision with 25 meV of GaN molecules. If a lasing device using exciton transitions was to be fabricated, ZnO molecules will have a superiority on GaN molecules supplied in which p-type conduction is achieved, and further essential processing abilities are improved for ZnO molecules. An additional encouraging implementation field of ZnO molecules is acoustic wave instrument because of their huge electromechanical coupling, especially through the c-plane. Additionally, ZnO molecules seem to be very suitable for growth of nano-scale structures, that can be utilized for electronic tool. An important section of the novel study in the area of ZnO-based electronic tools and implementations handle ZnO nanostructures and their integration with the general semiconducting materials for example Si, GaN, and other organic semiconducting materials. Morphology of ZnO nanowires has drawn great interest because of their great charge transporter features and good crystalline nature (Ozgur, Hofstetter, & Morkoç, 2010).

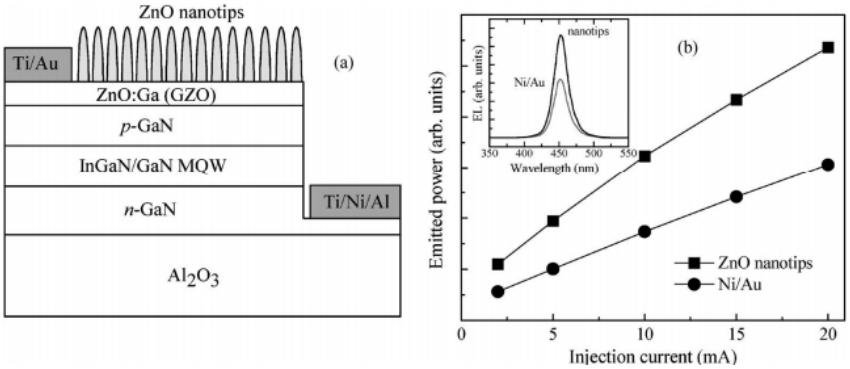

Figure 2.15 (a) Image of an integrated ZnO nanotip/GZO/GaN LED. (b) Light output power versus forward injection current for Ni/Au and ZnO nanotip/GZO/GaN LED (Zhong et al., 2007)

As illustrated Fig. 2.15(a), the Ga-doped ZnO (GZO) layer was placed above standard InGaN/GaN LED composition. After that, a bunch of ZnO nanotips was produced over GZO covered GaN as a layer where light extraction takes place. Compared to standard Ni/Au p-electrode GaN LED, the light emission efficiency was increased by 1.7 times [Fig. 2.15(b)]. Increasing in light extraction performance was clarified by the interactivity among the unplanned emission based on the GaN LED and ZnO nano-scale structures. The outcomes demonstrate that the cost-effective and extensive production strategies on the account of integration of ZnO nanotips with GaN-derived tools utilizing epitaxial production mechanism excluding the requirement for e-beam lithography or etching (Zhong et al., 2007).

2.4.3 Rubber Industry Application of ZnO

Worldwide manufacturing of ZnO number to over 100 tons yearly, and an important percentage is utilized by the rubber manufacturing to generate diverse dissimilar linked crossly rubber materials. The thermal conduction of ordinary silicone rubber is reasonably nominal; at the same time it can be enhanced by putting in specific thermal conduction fillers, containing inorganic and metal particles. Several sorts of thermal conduction particles, for example Al_2O_3, MgO, Al_2N_3, SiO_2, ZnO may enhance the thermal conduction of silicone-based rubber materials in the time of maintaining their excellent resistance to electricity. Therefore, these are encouraging materials as elevated efficiency engineering products. The integration of nano-scale fillers may obtain good thermal conductivity at a reasonably small filling content. ZnO molecules are a quite effectual and frequently utilized crossly linking chemical agent for elastomeric material which contain carboxyl group. The developed mechanical features of ionic elastomers mostly ensue from their great capability for stress relaxation, because of regeneration of electrovalent bond on exterior deterioration of the specimen. Furthermore, electrovalent bonded elastomeric materials have thermoplastic features also may be processed in a molten condition (Chatterjee & Naskar, 2007). On the other hand, there are several drawbacks to ZnO cross-linked elastomeric material which contain carboxyl group. A significant disadvantage is their weak flex features.

2.4.4 Textile Industry Application of ZnO

The garment sector presents a great chance for the marketing of nanomaterials. Especially, self-cleaning and water-resistant materials are extremely important for army implementations on the account of limited time for washing in critical circumstances. Furthermore, in the business community, water-resistant and self-cleaning materials are extremely beneficial for hindering unwanted spot on garments. Conservation of the body out of the detrimental UV part of sunbeam is an additional major field. Large number of researchers have been studying on UV-protective, water resistant and self-cleaning materials (Kolodziejczak-Radzimska & Jesionowski, 2014b). For garment implementation, not just are ZnO molecules organically appropriate, just as well nano-scale ZnO layer are greater air-permeable and effective as UV-blocking substance in comparison with bulkier equivalents of nano-scale ZnO molecules (Yadav et al., 2006). For this reason, ZnO nanostructured material have drawn attention as UV-blocker in garment coverings. Various methodologies have been published for the fabrication of UV-protective materials using ZnO nanostructured material. As example, hydrothermal produced ZnO nano-scale particles in SiO2-coated material displayed great UV-protective features (Mao, Shi, Zhang, & Cao, 2009).

The production of high profitable for example intelligent, medicinal and preventive materials has raised swiftly. The method to place nano-dimension coverings on materials for sensing and tracking function of the body, providing transmission service, delivering information and many other applications is examined seriously. ZnO is very common coating material to improve usefulness of textile products. ZnO powders are substances for a broad spectrum of implementations because oft their great optic, electronic and photocatalytic features. ZnO molecules are usually considered as a secure substance to people and other living organisms. Nano-scale ZnO molecules were the earliest substances utilized by consolidating they in sunbeam-protecting products (Rimbu et al., 2013).

CHAPTER THREE
EXPERIMENTAL PROCEDURE

3.1 Purpose

The main objective of this thesis could be categorized within 3 parts; the production, characterization and application of nanostructured ZnO. As already stated in previous sections,anodic oxidation process were used due to its cost-effectiveness and simple procedure. Based on the anodic oxidation parameters influence of structure and morphology on the optic, electronic and photocatalytic features are going to be investigated.

3.2 Materials

Bulk zinc (99% purity) was purchased from metal industry. $KHCO_3$ (99.7%), ethanol C_2H_5OH (≥ 99.9), acetone (C_3H_6O, 99.9%), H_2SO_4 (95-97%) and Na_2CO_3 (≥ 99.9 %) were supplied by Merck.

3.3 Production of ZnO Nanostructures

In this study, anodic oxidation method was utilized. Before anodic oxidation, a large piece of bulk Zn was cut off into 9 pieces with dimensions 3x3 cm^2. These pieces also named samples were performed to sanding process with different sandpaper. The samples were then sonicated in ethanol (C_2H_5OH), acetone (C_3H_6O) and deionized water in an ultrasonic tub for ten minutes separately. The anodic oxidation experiments were executed using the scheme (Fig. 3.1) containing sanded zinc plates as anode, platinum as cathode and $KHCO_3$ solutions as electrolyte. The anodic oxidation process was performed according to anodization parameters (Table 1) at room temperature. Produced ZnO samples were heat treated at 300 °C for 60 minutes with the heating rate of 5 °C/min.

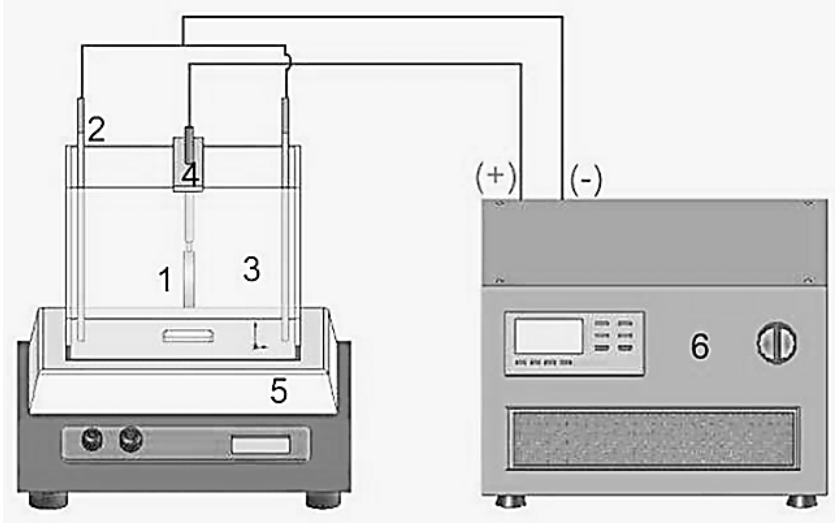

Figure 3.1 Diagrammatic representation of the electrochemical anodic oxidation (1) anode (2) cathode (3) electrolyte (4) anode holder (5) hot plate (6) power supply

Table 3.1 Parameters of anodic oxidation process

Sample	**Solution** (in H_2O)	**Voltage**	**Duration**
S1	0.05 M $KHCO_3$	20 V	30 min
S2	0.05 M $KHCO_3$	20 V	60 min
S3	0.05 M $KHCO_3$	20 V	120 min
S4	0.05 M $KHCO_3$	40 V	30 min
S5	0.05 M $KHCO_3$	40 V	60 min
S6	0.05 M $KHCO_3$	40 V	120 min
S7	0.05 M $KHCO_3$	60 V	30 min
S8	0.05 M $KHCO_3$	60 V	60 min
S9	0.05 M $KHCO_3$	60 V	120 min

3.4 Characterization of ZnO Nanostructures

Crystallographic structure of the samples was examined by an X-ray diffractometer (Thermo Scientific ARL X'TRA, XRD) with a Cu-K_α (1.54185 Å) irradiation. Diffraction patterns were collected at the scan rate of 2°/min in the 2θ range 5°–90° at standard ambient temperature as 25 °C. Scanning electron microscopy (SEM, Carl Zeiss 300VP) was operated to monitor the morphology and microstructure of the samples. The reduction of absorbance intensity of the methylene blue (MB) dye was observed utilizing the UV-Vis spectrophotometer (Shimadzu UV 1240 spectrophotometer) at 664 nm which matches the characteristic peak of MB. Elemental and survey analysis of ZnO specimens were examined by X-ray photoelectron spectroscopy (XPS, Thermo Scientific Al K-Alpha). The photocatalytic degradation of MB was studied under visible light source which was 300 W Osram Ultra-Vitalux E27 (4.3% UVA, 1% UVB, 94.47% Vis).

3.4.1 X-Ray Diffractometer (XRD)

X-ray diffraction technique is an effective non-contact process to identify phases in substances. It supplies data about natures of the materials as crystalline or amorphous. In addition to these, information of preferential orientation, particle size, crystalline, strain state, and defect structures are obtained by XRD. XRD peaks are generated by a monochromatic beam of X-rays scattered at specified gradients from every batch of lattice planes in a specimen. The peak intensity is identified through the position of atoms in the lattice planes. As a result, the XRD pattern is the mark of periodical atomic layouts for the material. Online library for XRD patterns allows swift phase detection for a wide range of crystalline specimens. Bragg's law is fundamental formula for XRD calculations:

$$n\lambda=2d\sin\theta \tag{3.1}$$

in which n is the order of diffraction, λ is the X-ray wavelength is the distance among scattering planes and θ is the angle amid the atomic planes and the incident X-ray beam

(Kohli & Mittal, 2019). Diffraction of x-rays via planes of atoms is demonstrated in figure 3.1.

X-ray beam is permitted to incident on a specimen, and reflected X-rays are identified by a detection device. XRD patterns are particular for the material under examination. XRD method is helpful in defining the percentage crystallinity pre- and post-treatment. In general, XRD peak of the specimen is registered on an X-ray diffractometer functioning at spesific potential and current at ambient temperature as 25 °C. Amorphous areas of the specimen generate wide peak, while crystalline areas generate strong peak. The level of crystallinity (X_C) is calculated by identifying the intensity of the crystalline phase (I_C) and amorphous phase (I_A) amounts inside the specimen (Patel & Parsania, 2017):

$$X_C = [I_C/(I_A+I_C)]\times 100 \quad (3.2)$$

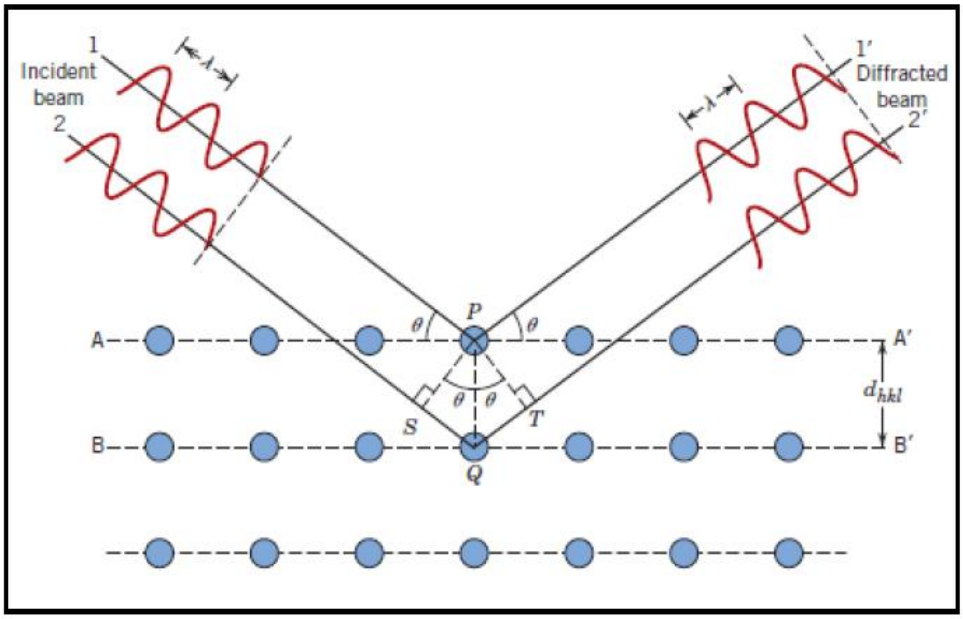

Figure 3.2 Diffraction of x-rays via planes of atoms (Erinosho, Collins, Wilkinson, Todd, & Dunne, 2016)

3.4.2 X-Ray Photoelectron Spectroscopy (XPS)

X-ray photoelectron spectroscopy, is the commonly utilized analytic method to display the surface chemistry of solid substances because of its clarity, elasticity, and reliable academic principle. XPS which is also named electron spectroscopy for element survey. The standard XPS mechanism consist of a super-high vacuum medium, X-ray origin, electron energy analyzing device, and information obtaining network. The specimen surface is treated by irradiation via monochromatic X-ray and the radiated photoelectrons are identified in XPS. Figure 3.3 explains the fundamental procedure of photoelectron genesis and the photoelectron energy is formulated as following:

$$E_b = \hbar v - KE \tag{3.4}$$

where KE is the kinetic energy of the radiated electron which is measured. E_b is generally stated in electron volts (eV). E_b is the electron binding energy in the atom, $\hbar v$ is the energy of the X-ray source (a given value in the experimentation). All elements generate a variety of individual peaks in the spectrum of photoelectrons. Additionally, peak intensity of elements is a straight value of the elemental composition. Because various electrons and a number of different binding energy exist in the nature of atom. Surface pollution can cause unexpected outcomes due to intensely surface sensitiveness of XPS. XPS analysis can be performed both qualitatively and quantitatively on whole elements excluding He and H. Moreover, the form of every peak intensities and the electron binding energies are able to be lightly changed through the chemical condition of the emitted atom. Therefore, XPS is able to also supply data about chemical bonds. (H. Wang & Chu, 2013).

XPS is the commonly utilized surface examination method owing to the fact that it may be implemented to a wide spectrum of substances and supplies important quantitative and chemical condition data from the outer layer of the substance being investigated. The standard deepness of survey for XPS measurements is about 5 nm.

The data XPS supplies regarding outermost layers is crucial for lots of manufacturing and experiment implementations where outermost layer performs a crucial part in effectiveness involving nano-scale materials, adhesion, corrosion, catalysis, photovoltaics, electrical equipments, magnetic medium, image technologies. XPS is a useful characterization device to investigate the surface of membranes. The scope of the elements is approved, and then contamination is detected. In addition to knowledgeable about the scope, it is likely to analyze the percentage of atomic composition (Aziz & Ismail, 2017).

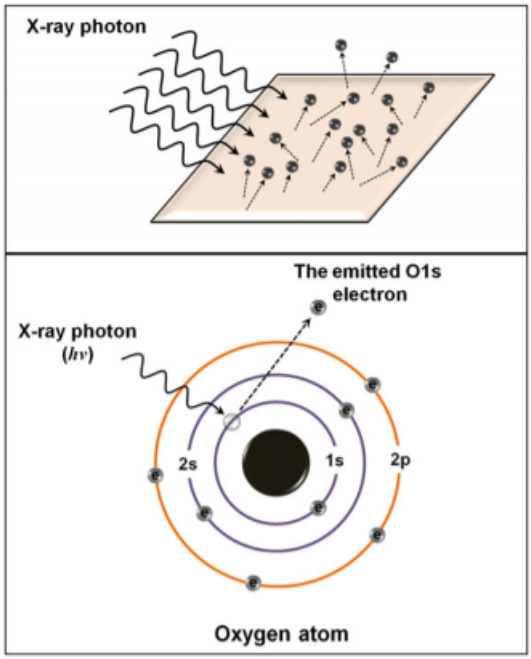

Figure 3.3 (Top) A surface exposed to irradiation via X-ray photons which leads emission of photoelectrons and (bottom) the X-ray photon transfers its energy to a core-level electron imparting sufficient energy for the electron to abandon the atom (H. Wang & Chu, 2013)

3.4.3 Scanning Electron Microscopy (SEM)

Scanning electron microscopy (SEM) is broadly utilized to examine a variety of materials microstructural and chemical. The essential instruments of the SEM contain a source of electrons, electromagnetic lenses to focalize electrons, electron detectors,

specimen chambers, software and monitors to observe the displays (Figure 3.2). Electrons, generated at the top of the column, are speeded up towards the bottom where they crossed over a partnership of lenses and holes to generate a thin beam of electrons. The electron beam strikes the exterior of the sample assembled on a flexible platform in vacuum. The specimen exterior is detected by movement of the beam coils. This beam detecting allows data about a determined field of the specimen. The cooperation of the electron beam by the specimen generates a variety of signals, which can then be defined by suitable detecting devices. The benefits of SEM contain the elaborate three-dimensional (3D) image of topography and the all-around data supplied from dissimilar detecting devices. The microscope is simple to function, and related software is uncomplicated. The drawbacks of SEM are its largeness and price. SEM is costly to function. The arrangement of specimens can cause defects. A major drawback is that SEM is restricted to solid, inorganic specimens relatively minor to place interior a vacuum chamber (Singh, 2016).

SEM displays the specimen surface via examining it in the company of an intense energy electron beams in a raster scanning model. The primary electron beam, which is generated under high vacuum, is examined over the entire area of a sample. When the electrons hit the sample, an assortment of the signal generate a view of the surface with energy dispersive X-rays (EDX). Various features have been advanced by the fundamentals of SEM to have a greater knowledge of substance surfaces. Back scattered electrons (BSE) are mirrored from the specimen via elastic interactions between the beam and the sample. BSE displays may supply data on the subject of the distribution of various elements in the specimen as reported by their atomic number (Yan, 2010).

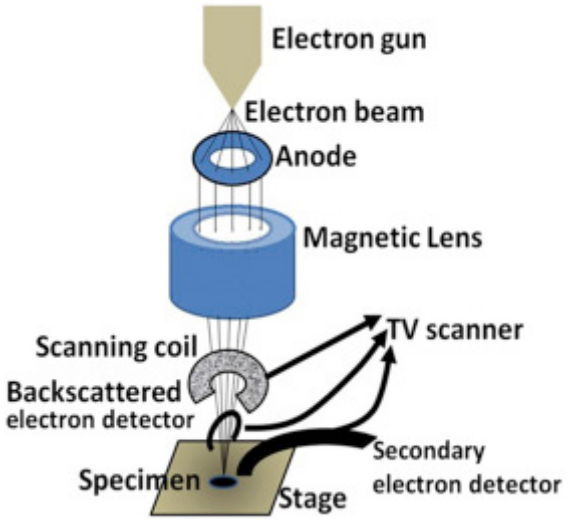

Figure 3.4 Schematic of smayning electron microscopy(SEM) system (Singh, 2016)

3.4.4 UV-Vis Spectrophotometer

The word 'spectroscopy' includes a variety of methods for obtaining data about structures of atoms and molecules. Under all circumstances, emission, scattering, or absorption of radiation exist, on the other hand the fundamental procedures by which these happen vary significantly, as does the essence of the data that may be acquired. Radiation is absorbed by the excitation of electrons among their energy levels in UV/VIS spectroscopy. This can happen for atoms in addition to molecules. Electrons inside particles are deemed to present in orbitals of the molecules, that may be non-bonding, antibonding, or bonding orbitals. As a result, the transitions among energy states may be explained as molecular orbital transitions of the particle. The region of the particle where leads to electronic absorptions is recognized as a chromophore. Chromophore electrons which engaged in the transition are the non-bonding outer electrons of having high electronegativity for example sulfur, oxygen, or nitrogen, or they are directly utilized in bond formation (McLaughlin & Glennon, 2011).

The association among concentration and absorbance is referred to as Beer's law (also known as Bouguer–Lambert–Beer law) and is explained via the formula:

$$A=\varepsilon bc \quad (3.3)$$

Where b is the path length of radiation across the absorbing environment, ε is the molar absorptivity, A is the absorbance of the solution, and c is the concentration. The fundamental mechanism includes a radiation origin, a selection instrument for wavelength, a specimen chamber, a detecting device and an output instrument. While, deuterium lamps are generally utilized for near-UV radiation, tungsten filaments are the more frequent sources for visible radiation. For cost-effective origin with low bandwidths (generally 20–30 nm), light emitting diodes may be utilized. UV–visible spectrophotometry is primarily utilized for the quantitative definition of organic and inorganic components in a broad spectrum of specimen matrices, such as, ecological, biochemical, medical. UV/VIS spectroscopy method may be utilized on the account of the straight identification of absorbing species, but caution must be taken to prevent matrix interventions. Reaction speed calculations, utilized in procedures which are depended on catalytic reactions, may accomplish such interventions and supply good sensitiveness (Worsfold, 2004).

10^{-5} M (3.2 mg/L) MB dye was arranged in order to observe photocatalytic performance of the ZnO nanostructures. ZnO nanostructures which were considered as a catalyst, were put into beakers which contained 40 ml of MB dye with the help of twezeer. Additionally, a catalyst-free sample was investigated in order to contrast with the outcome acquired from catalyzed samples. The space among the UV light origin and beakers was 15 cm for all samples. In the experiment, 3 ml of liquid from the beakers was extracted transitorily at 60^{th}, 120^{th}, 180^{th}, 240^{th} ,300^{th}, 360^{th}, and 420^{th} minutes. The observed absorbance datas were transformed to concentration datas utilizing the Bouguer–Lambert–Beer law. Degradation performance of ZnO nanostructures was expressed by the formula:

$$DE=[(C_0 - C_f)/C_0] \times 100 \quad (3.4)$$

Where C_f is final concentration, C_0 is beginning concentration and DE is degradation efficiency. Additionally, the photocatalytic degradation rate was computed for all samples utilizing by the formula:

$$\ln \frac{C_0}{C} = kt \tag{3.5}$$

As mentioned earlier, C is the concentration of MB at any time t, C_0 is the initial concentration of MB and the rate of degradation was shown as k.

CHAPTER FOUR

RESULTS AND DISCUSSION

4.1 Phase Analysis

In the XRD pattern of the produced ZnO samples on the zinc plates as shown in Figure 4.1, the peaks were detected at 31°, 34°, 36°, 47°, 56° and 63° corresponding to the (100), (002), (101), (102), (110) and (103) polycrystalline planes of ZnO (Ponja, Sathasivam, Parkin, & Carmalt, 2020). It has been observed that peaks in all produced films belong to the hexagonal wurtzite structure of ZnO (ICDD 36-1451). In addition, peak intensities of the Zinc substrate were detected in the XRD patterns of some specimens. These peak intensities corresponding to hexagonal structure of the Zinc metal with ICDD card number of 87-0713(Ashok Kumar & Sammaiah, 2018). XRD patterns of all produced anodic films are broadly in agreement with the outcomes acquired formerly by some researchers (Basnet, Samanta, Inakhunbi Chanu, Mukherjee, & Chatterjee, 2019; Mika et al., 2019).

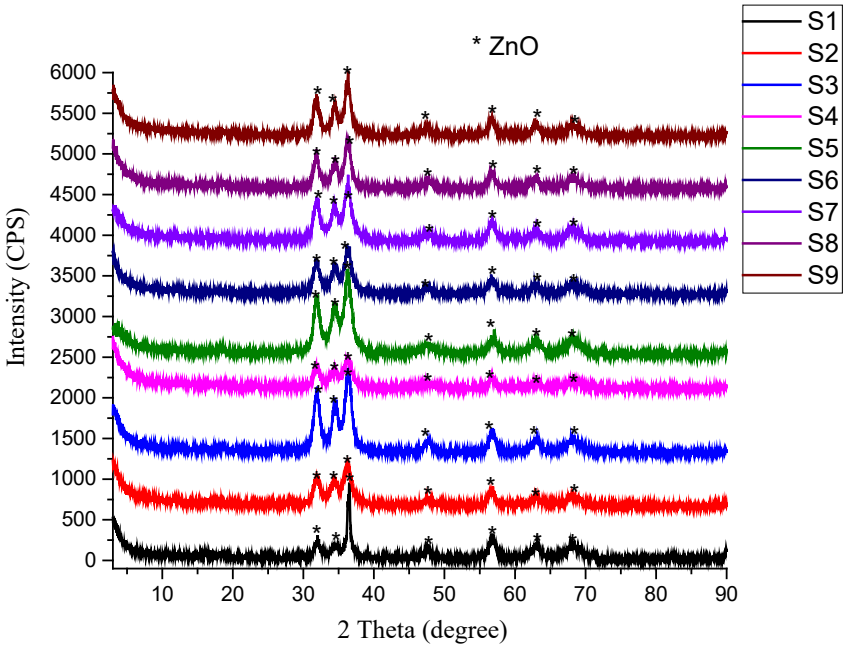

Figure 4.1 XRD patterns of ZnO samples

4.2 XPS Results

Elemental analyses of ZnO samples were executed with the help of XPS. The samples coded S1, S2, S3, S4, S5, S6, S7, S8 and S9 were elementally surveyed considering and the results were displayed in Figures 4.2, 4.3, 4.4, 4.5, 4.6, 4.7, 4.8, 4.9 and 4.10 respectively. It was observed that zinc is the primary elemental component of the plates in Zn2p form. The C1s peak seen in the ZnO samples belong to the usage of the $KHCO_3$ solution as an electrolyte in anodic oxidation process. Elemental XPS spectra of Zn 2p and O 1s of all samples are shown in Figures 4.11 and 4.12. The XPS spectrum of ZnO gives the characteristic peak intensities of Zn 2p, O 1s and C 1s with the in order of corresponding binding energies of 1022, 531 and 285 eV approximately. Furthermore, the high-resolution Zn 2p spectrum for ZnO samples (Figure 4.11) showed two remarkable peaks with binding energies of approximately 1022 and 1045 eV, matching to Zn 2p3/2 and Zn 2p1/2 respectively and is in agreement with the published articles (Haldorai, Voit, & Shim, 2014; Ramírez-Amador et al., 2020).

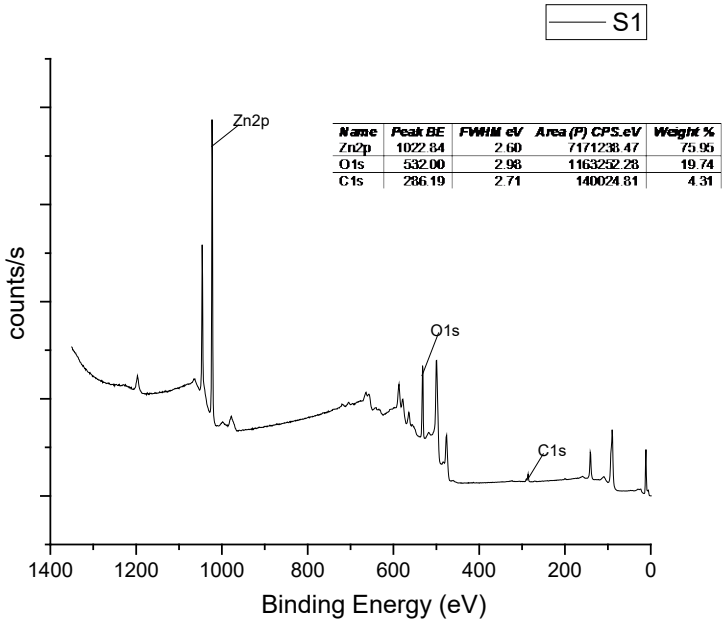

Name	Peak BE	FWHM eV	Area (P) CPS.eV	Weight %
Zn2p	1022.84	2.60	7171238.47	75.95
O1s	532.00	2.98	1163252.28	19.74
C1s	286.19	2.71	140024.81	4.31

Figure 4.2 XPS result of S1

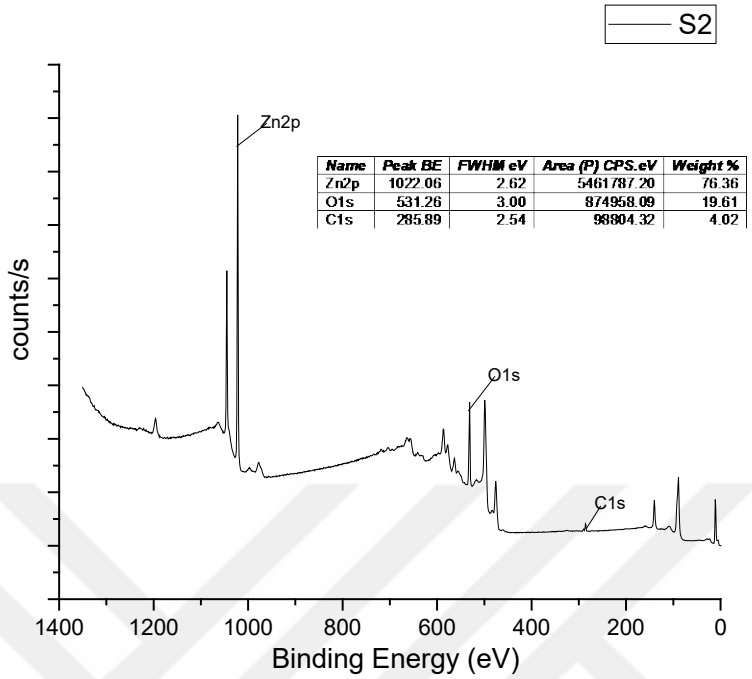

Name	Peak BE	FWHM eV	Area (P) CPS.eV	Weight %
Zn2p	1022.06	2.62	5461787.20	76.36
O1s	531.26	3.00	874958.09	19.61
C1s	285.89	2.54	98804.32	4.02

Figure 4.3 XPS result of S2

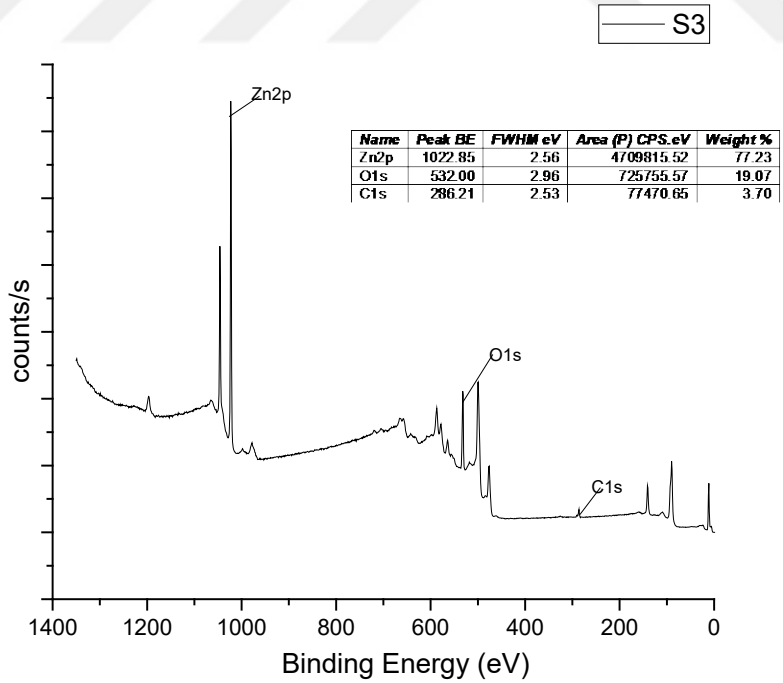

Name	Peak BE	FWHM eV	Area (P) CPS.eV	Weight %
Zn2p	1022.85	2.56	4709815.52	77.23
O1s	532.00	2.96	725755.57	19.07
C1s	286.21	2.53	77470.65	3.70

Figure 4.4 XPS result of S3

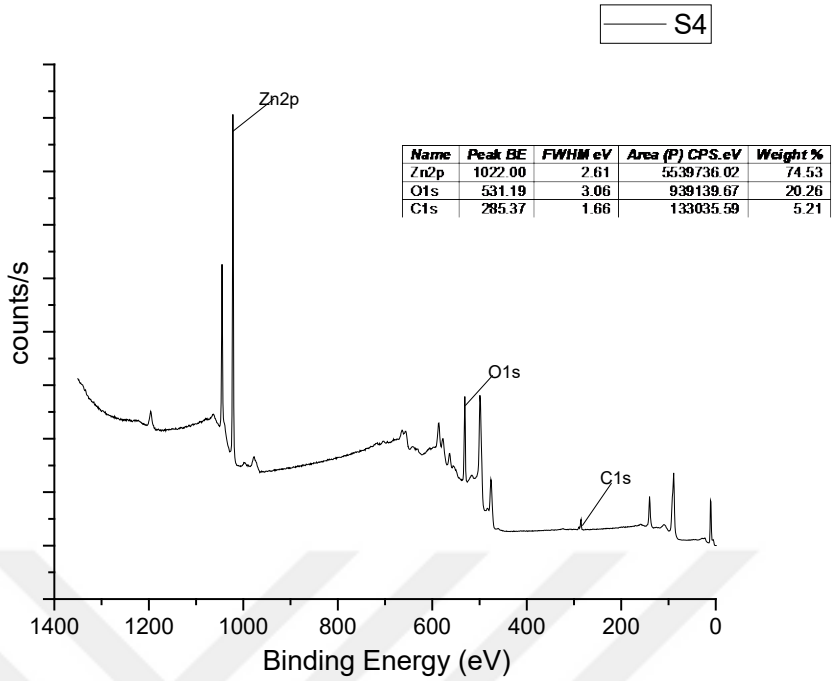

Name	Peak BE	FWHM eV	Area (P) CPS.eV	Weight %
Zn2p	1022.00	2.61	5539736.02	74.53
O1s	531.19	3.06	939139.67	20.26
C1s	285.37	1.66	133035.59	5.21

Figure 4.5 XPS result of S4

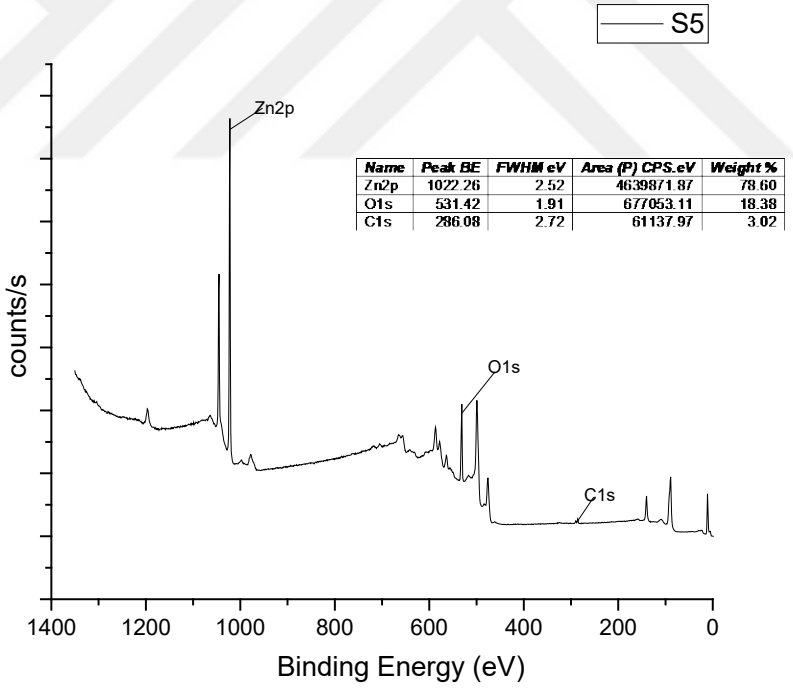

Name	Peak BE	FWHM eV	Area (P) CPS.eV	Weight %
Zn2p	1022.26	2.52	463987.87	78.60
O1s	531.42	1.91	677053.11	18.38
C1s	286.08	2.72	61137.97	3.02

Figure 4.6 XPS result of S5

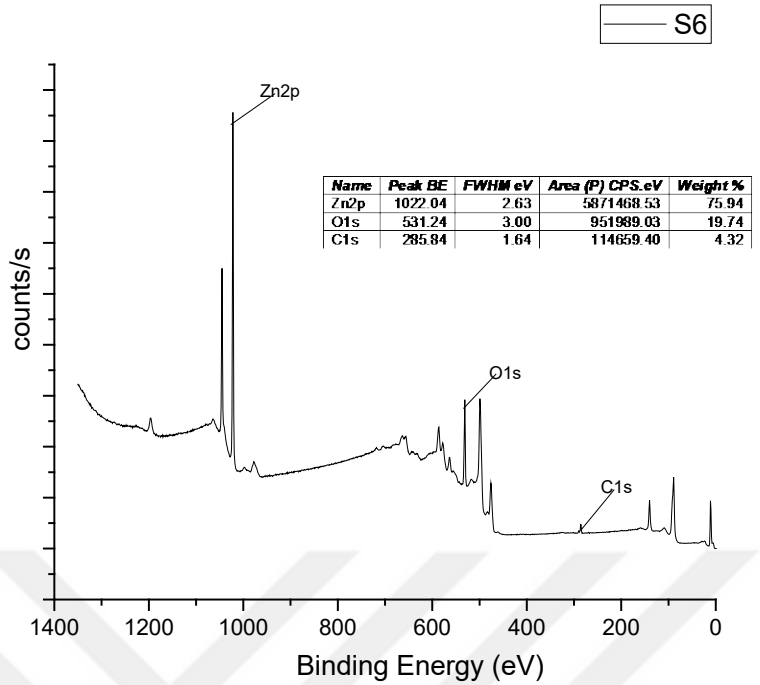

Name	Peak BE	FWHM eV	Area (P) CPS.eV	Weight %
Zn2p	1022.04	2.63	5871468.53	75.94
O1s	531.24	3.00	951989.03	19.74
C1s	285.84	1.64	114659.40	4.32

Figure 4.7 XPS result of S6

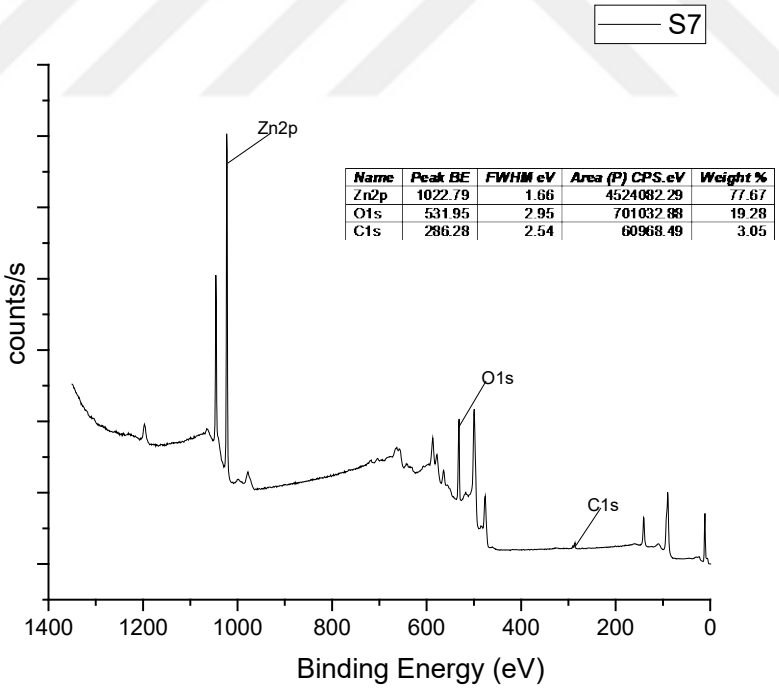

Name	Peak BE	FWHM eV	Area (P) CPS.eV	Weight %
Zn2p	1022.79	1.66	4524082.29	77.67
O1s	531.95	2.95	701032.88	19.28
C1s	286.28	2.54	60968.49	3.05

Figure 4.8 XPS result of S7

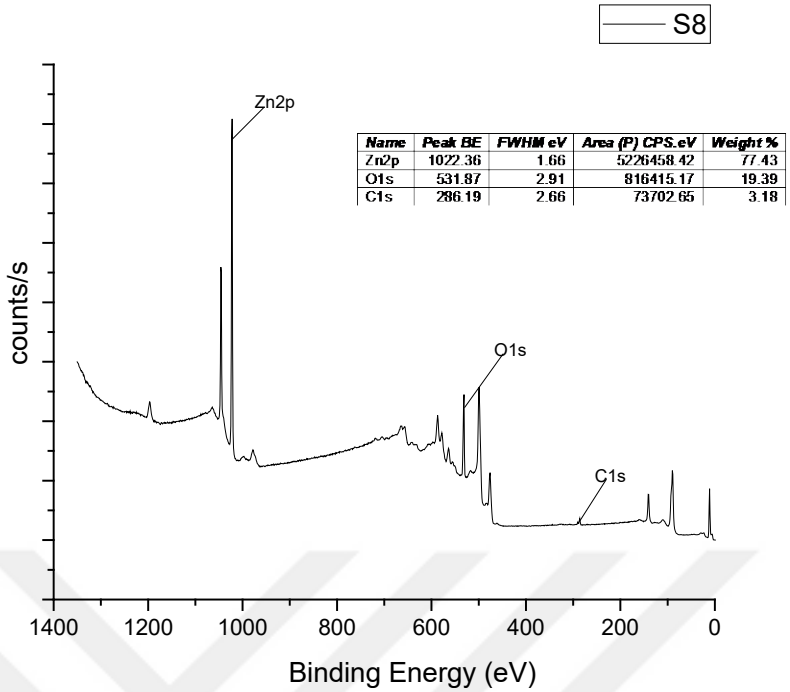

Name	Peak BE	FWHM eV	Area (P) CPS.eV	Weight %
Zn2p	1022.36	1.66	5226458.42	77.43
O1s	531.87	2.91	816415.17	19.39
C1s	286.19	2.66	73702.65	3.18

Figure 4.9 XPS result of S8

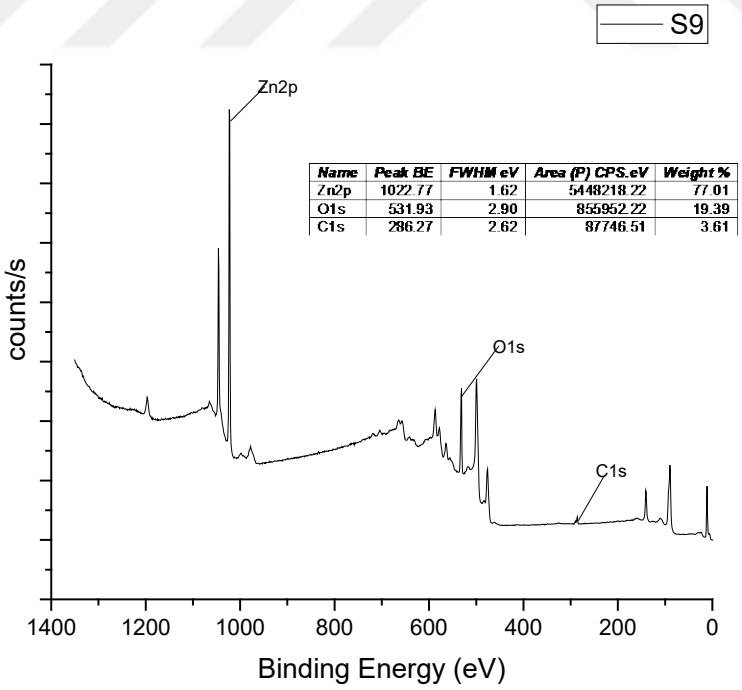

Name	Peak BE	FWHM eV	Area (P) CPS.eV	Weight %
Zn2p	1022.77	1.62	5448218.22	77.01
O1s	531.93	2.90	855952.22	19.39
C1s	286.27	2.62	87746.51	3.61

Figure 4.10 XPS result of S9

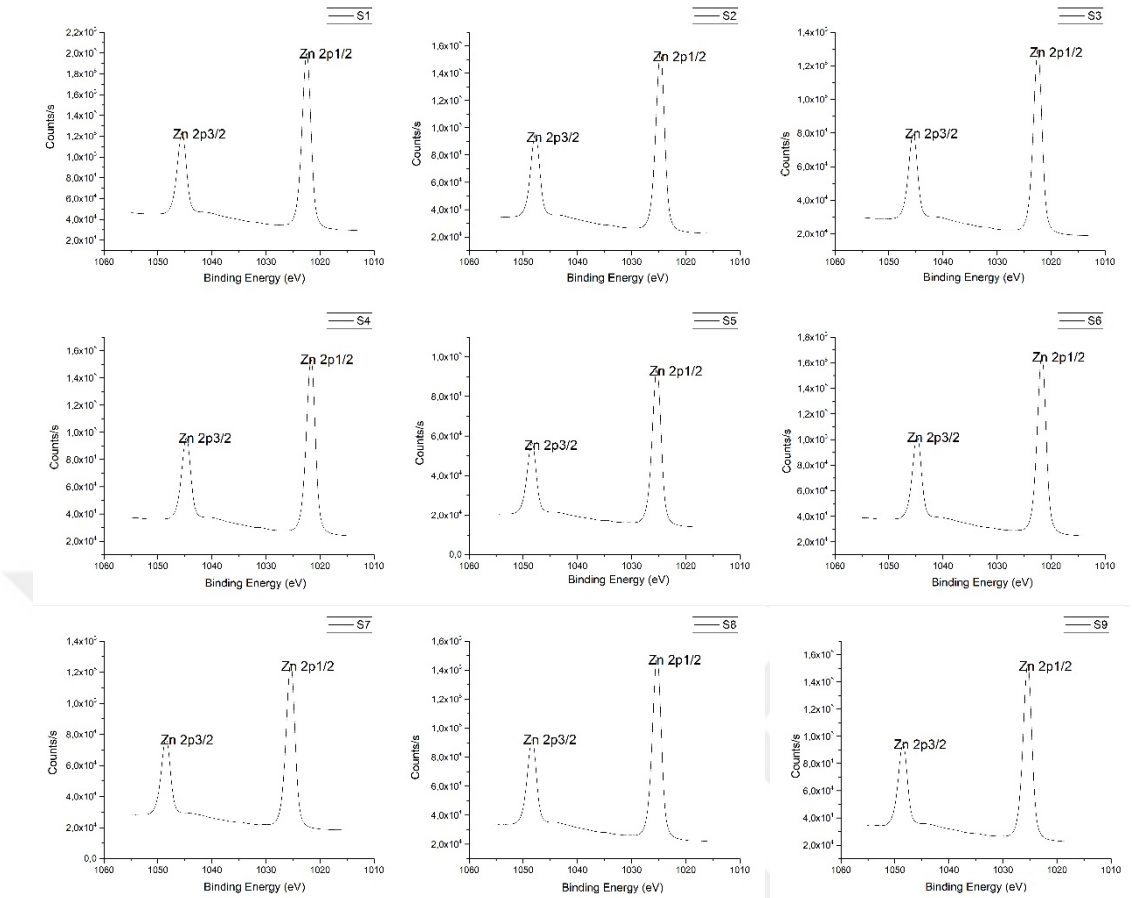

Figure 4.11 Zn 2p1/2 and Zn 2p3/2 spectrum for ZnO samples

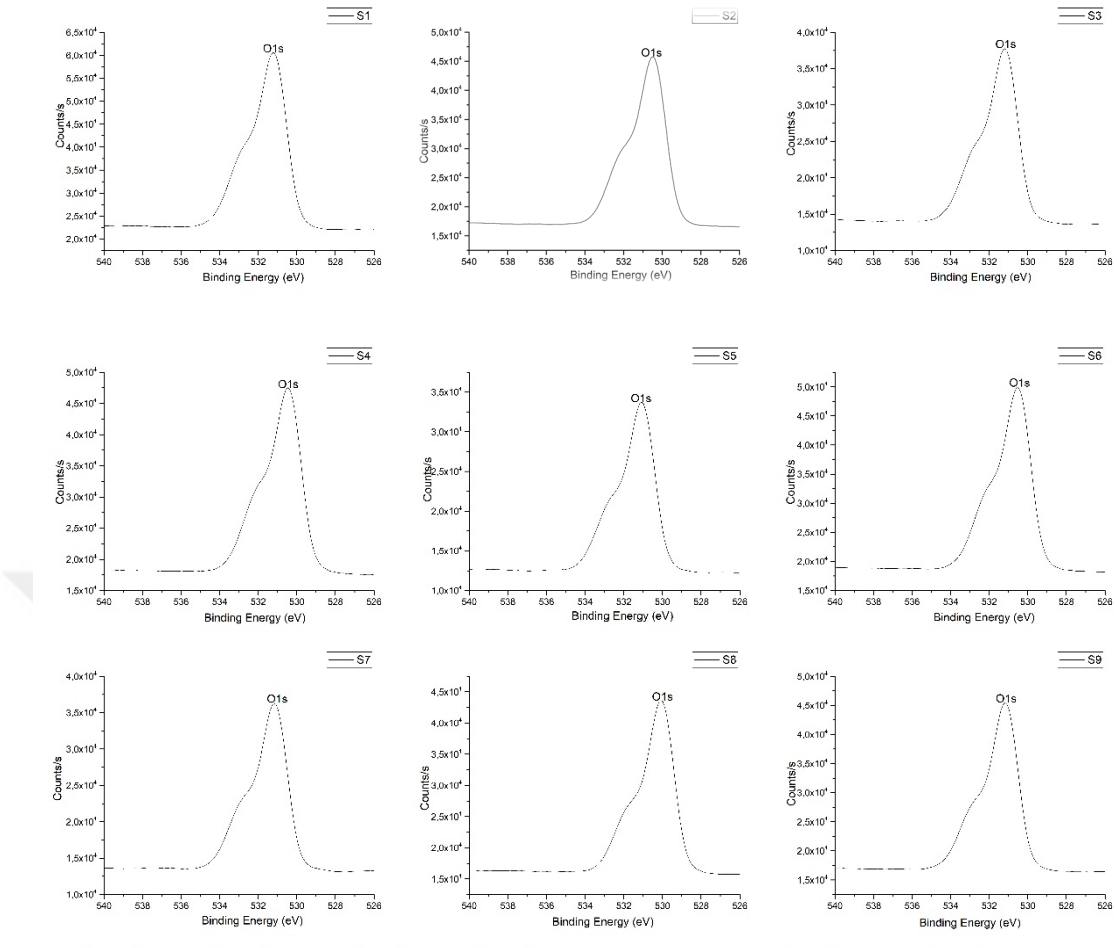

Figure 4.12 O 1s spectrum for ZnO samples

4.3 SEM Results

In the interest to investigate the surface features of the anodized ZnO samples SEM analysis were performed and presented in Figures 4.14, 4.15 and 4.16 at different magnifications (5k and 30k). The anodization parameters of samples which were used in the experiment given in Table 3.1. Electron micrographs of samples S1, S2 and S3 were given in Figure 4.14 at 5k magnification for general view and 30k magnification for detail view at 20V. It is clearly seen that while the other parameters are constant(voltage, ph, solution concentration etc.), the nanowires tips become clumped as the duration increases in Figure 4.14. SEM images of samples S4, S5 and S6 were demonstrated in Figure 4.15 at 40V. It may be stated that 40V is more appropriate for production of ZnO nanowires compared to 60V. SEM photographs of samples S7, S8

and S9 were displayed in Figure 4.16 at 5k and 30k magnification at 60V. It may be concluded that the agglomeration of nanowires increases signifimaytly as the anodizing time increases at high voltage(60V). In addition, flower-like nanostructures was observed in Figure 4.13. Consequently, it may be expressed that the homogeneous and dense distribution of ZnO nanowires are appeared in all samples except of S8 and S9. This indicates that voltage and duration have a signifimayt influence on formation of the uniform ZnO nanowires.

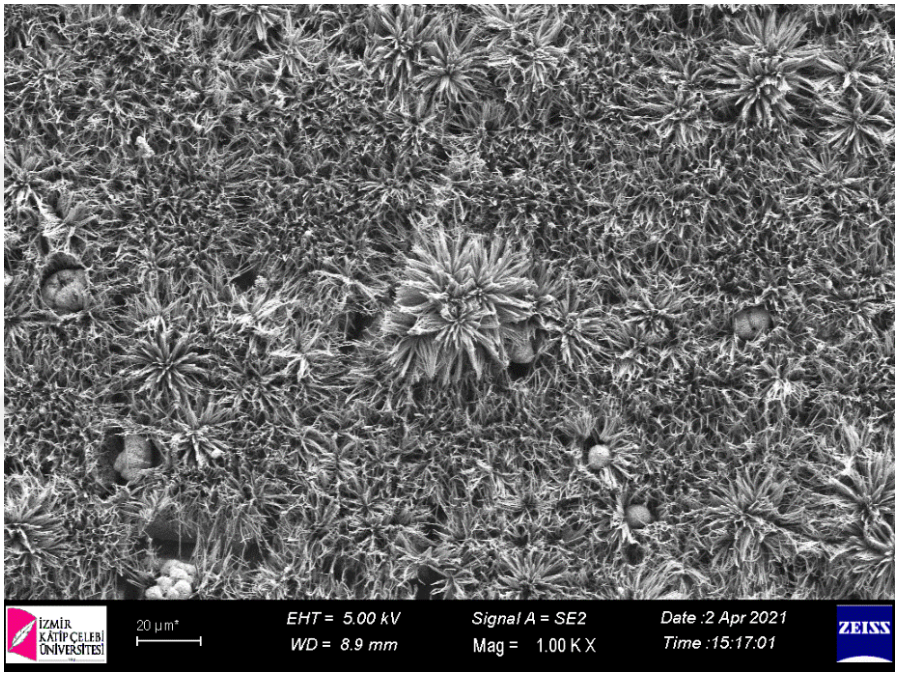

Figure 4.13 SEM images of the sample S4 at 1k magnification

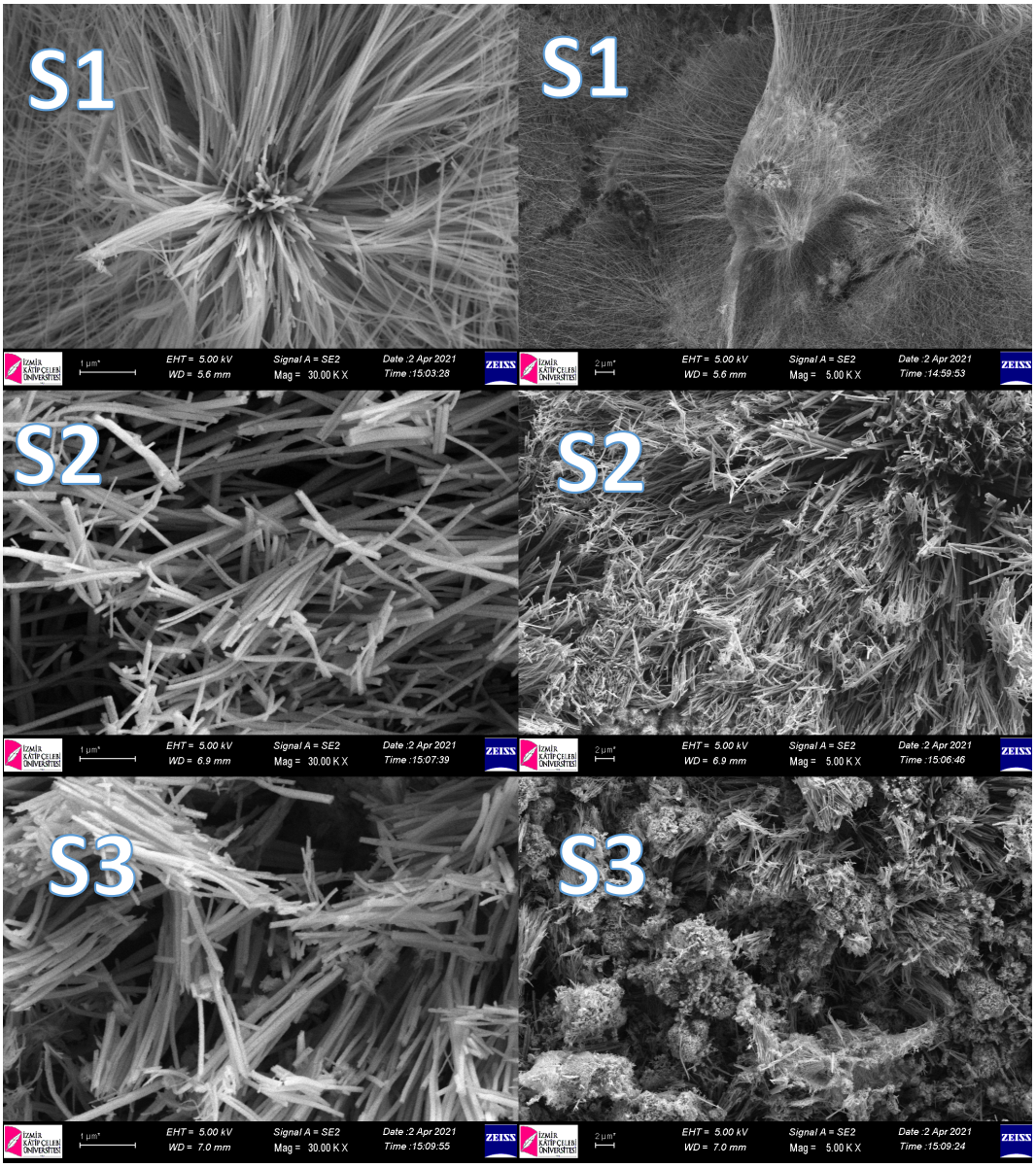

Figure 4.14 SEM images of the sample S1,S2 and S3(The images on the right side of the figure were taken at 5K magnification, and the ones on the left at 30K)

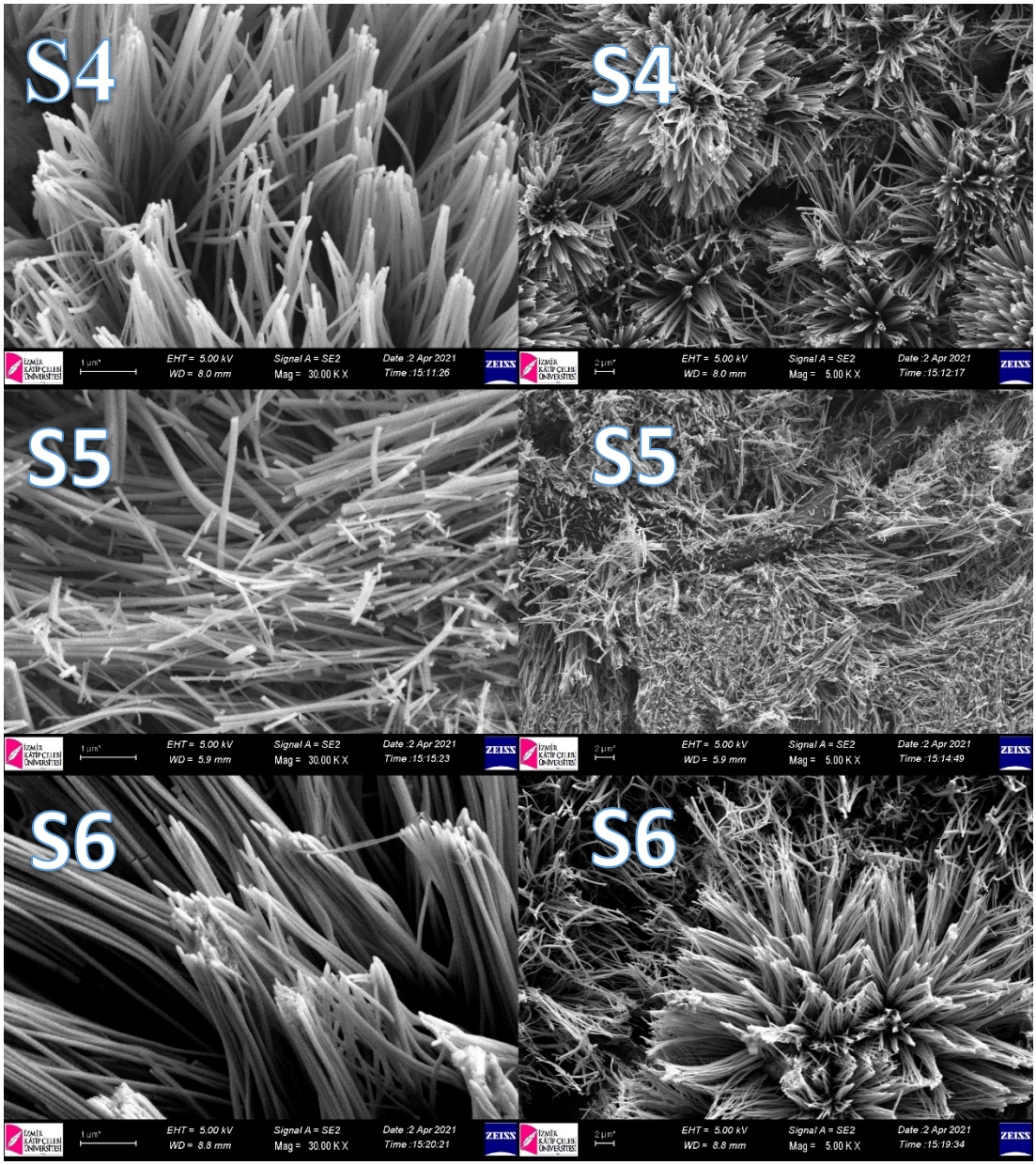

Figure 4.15 SEM photographs of samples S4, S5 and S6 (The images on the right side of the figure were taken at 5K magnification, and the ones on the left at 30K)

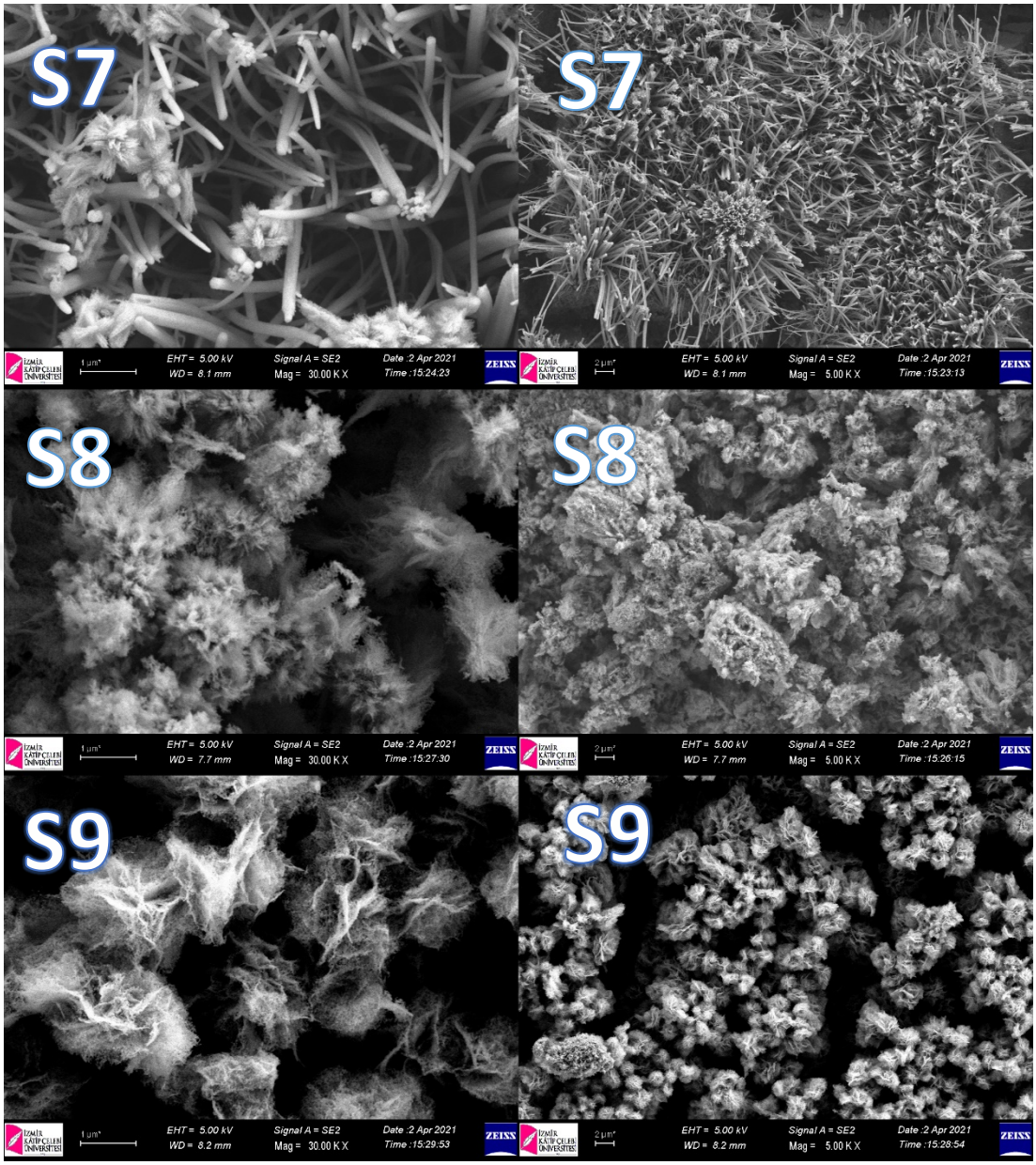

Figure 4.16 . Electron micrographs of samples S7, S8 and S9 (The images on the right side of the figure were taken at 5K magnification, and the ones on the left at 30K)

4.4 Photocatalytic Activity

Photocatalytic performances of ZnO samples added into 10^{-5} M MB were evaluated by measuring the absorbance data of MB at specific periods of time. Photocatalysts break down MB solution by the period of time due to photocatalytic effect and then cause its color to be removed. Concentration information were acquired based on the

absorbance intensities of the characteristic peak of MB at 664 nm utilizing the Lambert-Beer law.. Figure 4.17a shows the change in concentration of MB for 420 minutes. The variation of the obtained ln(C_0/C) values over time was shown in Figure 4.17b. It was determined that these values were compatible with the first order Lambert-Beer law.

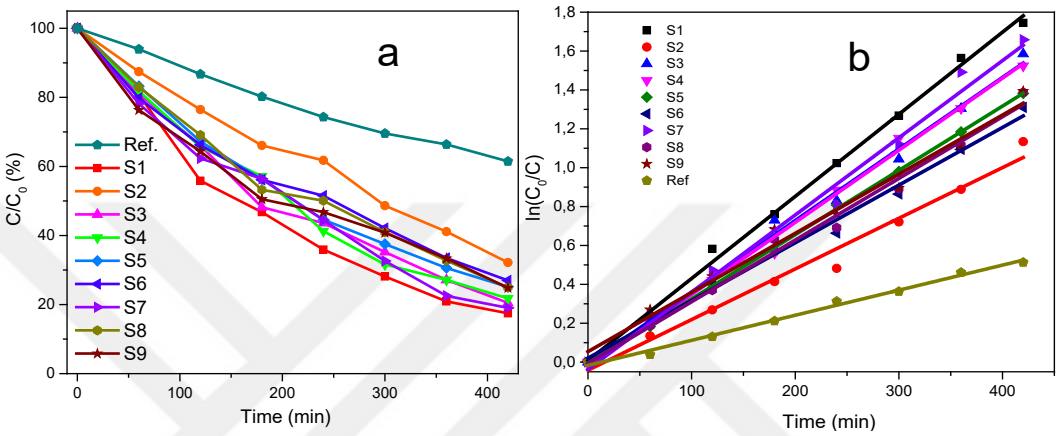

Figure 4.17 Photocatalytical performances of ZnO samples for different anodization times

There are many factors affecting photocatalytic performance for example phase composition, surface area, crystallinity and morphology (Dikici et al., 2015). The degradation efficiencies of MB by different samples were calculated according to the beginning absorbance intensity of 0.693 at 664 nm. These results were indicated in the bar chart in Figure 4.18. As may be seen from Figure 4.18, the S1 sample has the greatest photocatalytic effectiveness owing to 82.5% degradation efficiency in 420 minutes. where arbitration sample was 38.5%. As another observation, the photocatalytic performance was affected by changing the anodization time, voltage, and electrolyte.

The absorption spectra of MB for the S1 sample was created for different durations and was shown in Figure 4.19. MB was degraded for 420 minutes under UV-Vis light source using the S1 sample. The absorbance intensity of MB was reduced from 0.693 to 0.121 at 664 nm in the asset of S1 specimen beneath UV-Vis light illumination for 420 minutes.

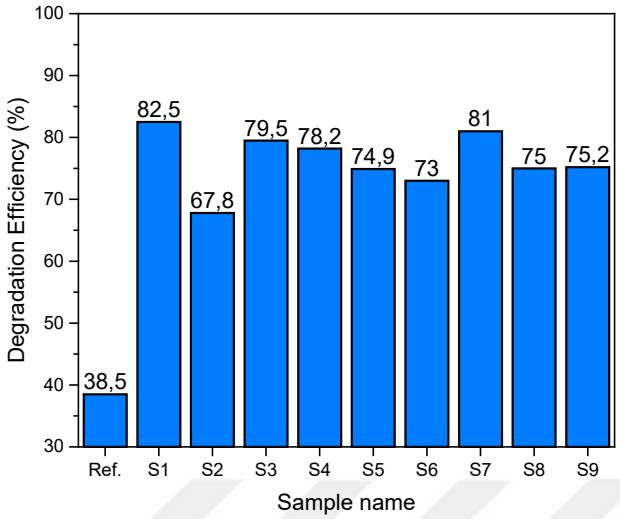

Figure 4.18 Photocatalytic degradation efficiencies of MB by different samples under UV irradiation

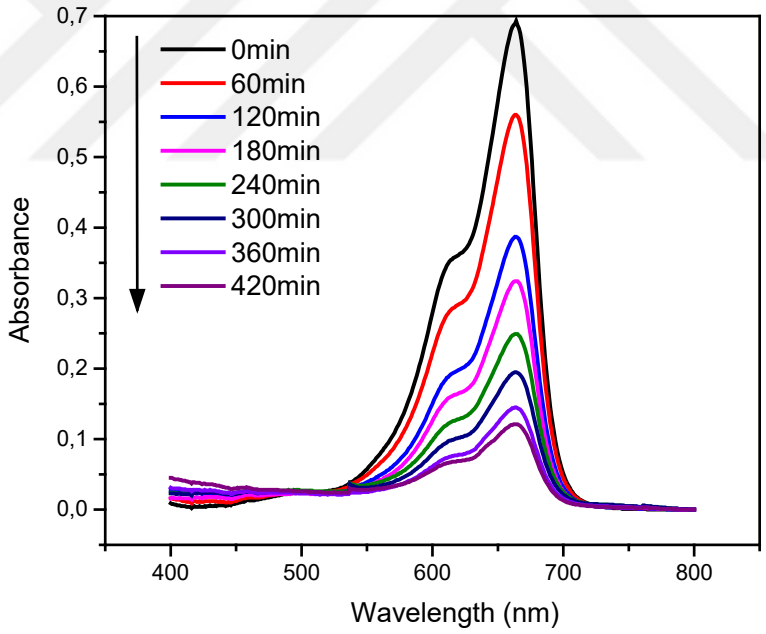

Figure 4.19 UV absorption spectra of the MB for S1 sample after UV–Vis light illumination

CHAPTER FIVE
CONCLUSION AND FUTURE WORKS

Synthesis and characterization of nanostructured ZnO were performed without any inaccuracy. In addition to these, possible applications of nanostructured ZnO were presented. In advance of anodic oxidation, bulk Zn samples divided in nine part and then sanded up to make smooth material surface. ZnO samples were grown by anodic oxidation method. After that, the nano-scale ZnO samples were heat treated at 300 °C for one hour with the heating rate of 5 °C/minute. The acquired data from XRD analysis macthed with characteristic peak of ZnO. Also, elemental XPS spectra of Zn 2p and O 1s of nanostructured ZnO samples compromise with fingerprint peaks of Zn 2p, O 1s and C 1s with the in order of corresponding binding energies of 1022, 531 and 285 eV approximately. Moreover, the high-resolution Zn 2p spectrum for nanostructured ZnO samples demonstrated two noteworthy peaks with binding energies of in the region of 1022 and 1045 eV matching to Zn 2p3/2 and Zn 2p1/2 respectively. According to these informations XPS survey confirmed that chemical composition of the samples was ZnO. Morphology of nanostructured ZnO samples were observed as nanowires except of coded samples S8 and S9 with the assistance of SEM. As a result of long period of anodic oxidation with high potentials(40V and 60V) caused agglomeration of nanowires in samples S8 and S9. Photocatalytic performances of ZnO samples added into 10-5 M MB were analyzed by metering the absorbance information of MB at spesific time intervals. The degradation efficiencies of MB were calculated according to the first absorbance value of 0.693 at 664 nm. The absorbance values of MB was decreased gradually at 664 nm in the presence of nanostructured ZnO samples under UV-Vis light illumination for 420 minutes.

REFERENCES

Angus Macleod, H. (2013). Recent developments in deposition techniques for optical thin films and coatings. In *Optical Thin Films and Coatings: From Materials to Applications,* 3–25

Ashok Kumar, V., & Sammaiah, P. (2018). Comparison of process parameters ınfluence on mechanical and metallurgical properties of zinc coating on mild steel & aluminium during mechanical process. *Materials Today: Proceedings*, *5*, 3861–3866.

Aziz, M., & Ismail, A. F. (2017). X-Ray photoelectron spectroscopy (XPS). In *Membrane Characterization*, 81–93.

Basnet, P., Samanta, D., Inakhunbi Chanu, T., Mukherjee, J., & Chatterjee, S. (2019). Assessment of synthesis approaches for tuning the photocatalytic property of ZnO nanoparticles. *SN Applied Sciences*, *1*, 1–13.

Behera, A., Mallick, P., & Mohapatra, S. S. (2020). Nanocoatings for anticorrosion. In *Corrosion Protection at the Nanoscale* 227–243.

Chatterjee, K., & Naskar, K. (2007). Development of thermoplastic elastomers based on maleated ethylene propylene rubber (m-EPM) and polypropylene (PP) by dynamic vulcanization. *Express Polymer Letters*, *1*, 527–534.

Chhipa, H. (2019). Mycosynthesis of nanoparticles for smart agricultural practice: A green and eco-friendly approach. In *Green Synthesis, Characterization and Applications of Nanoparticles*, 87–109.

Dal Corso, A., Posternak, M., Resta, R., & Baldereschi, A. (1994). Ab initio study of piezoelectricity and spontaneous polarization in ZnO. *Physical Review B*, *50*, 10715–10721.

Dikici, T., Yildirim, S., Yurddaskal, M., Erol, M., Yigit, R., Toparli, M., & Celik, E. (2015). A comparative study on the photocatalytic activities of microporous and nanoporous TiO2 layers prepared by electrochemical anodization. *Surface and Coatings Technology*, *263*, 1–7.

Dong, J., Liu, Z., Dong, J., Ariyanti, D., Niu, Z., Huang, S., & Gao, W. (2016). Self-organized ZnO nanorods prepared by anodization of zinc in NaOH electrolyte. *RSC Advances*, *6*, 72968–72974.

Erinosho, T. O., Collins, D. M., Wilkinson, A. J., Todd, R. I., & Dunne, F. P. E. (2016). Assessment of X-ray diffraction and crystal plasticity lattice strain evolutions under biaxial loading. *International Journal of Plasticity*, *83*, 1–18.

Faraji, G., Kim, H. S., & Kashi, H. T. (2018). Introduction. In *Severe Plastic Deformation*, 1–17

Ferreira, F. V., Franceschi, W., Menezes, B. R. C., Biagioni, A. F., Coutinho, A. R., & Cividanes, L. S. (2019). Synthesis, characterization, and applications of carbon nanotubes. In *Carbon-Based Nanofillers and Their Rubber Nanocomposites: Carbon Nano-Objects*, 1–45.

France, J. L., Cain, M., Fisher, R. E., Lowry, D., Allen, G., O Shea, S. J., & Nisbet, E. G. (2016). Identifying sources of arctic methane. *Journal of Geophysical Research: Atmospheres*, *121*, 14,257-14,270.

Goh, H. S., Adnan, R., & Farrukh, M. A. (2011). ZnO nanoflake arrays prepared via anodization and their performance in the photodegradation of methyl orange. *Turkish Journal of Chemistry*, *35*, 375-391.

Haldorai, Y., Voit, W., & Shim, J. J. (2014). Nano ZnO@reduced graphene oxide composite for high performance supercapacitor: Green synthesis in supercritical fluid. *Electrochimica Acta*, *120*, 65–72.

Hernández Battez, A., González, R., Viesca, J. L., Fernández, J. E., Díaz Fernández, J. M., Machado, A., & Riba, J. (2008). CuO, ZrO2 and ZnO nanoparticles as antiwear additive in oil lubricants. *Wear*, *265*, 422–428.

Kafle, B. P. (2020). Introduction to nanomaterials and application of UV–Visible spectroscopy for their characterization. In *Chemical Analysis and Material Characterization by Spectrophotometry*, 147–198.

Kato, H., Sano, M., Miyamoto, K., & Yao, T. (2002). Growth and characterization of Ga-doped ZnO layers on a-plane sapphire substrates grown by molecular beam epitaxy. *Journal of Crystal Growth*, *237–239*, 538–543.

Klingshirn, C. (2007). ZnO: Material, physics and applications. *ChemPhysChem*, *8*, 782–803.

Kohli, R. R., & Mittal, K. L. (2019). Methods for assessing surface cleanliness. In *Developments in Surface Contamination and Cleaning, 12*, 23–105.

Kolodziejczak-Radzimska, A., & Jesionowski, T. (2014a). Zinc oxide-from synthesis to application: A review. *Materials*, *7*, 2833–2881.

Kolodziejczak-Radzimska, A., & Jesionowski, T. (2014b). Zinc oxide-from synthesis to application: A review. *Materials*, *7*, 2833–2881.

Kudo, A., & Miseki, Y. (2009). Heterogeneous photocatalyst materials for water splitting. *Chemical Society Reviews*, *38*, 253–278.

Li, X., Yu, J., & Jaroniec, M. (2016). Hierarchical photocatalysts. *Chemical Society Reviews*, *45*, 2603–2636.

Li, Z., & Aik Khor, K. (2019). Preparation and properties of coatings and thin films on metal implants. In *Encyclopedia of Biomedical Engineering* 1–3, 203–212.

Litton, C. W., Reynolds, D. C., & Collins, T. C. (2011). Zinc oxide materials for electronic and optoelectronic device applications. In C. W. Litton, D. C. Reynolds, & T. C. Collins (Eds.), *Zinc Oxide Materials for Electronic and Optoelectronic Device Applications*. Chichester, UK: John Wiley & Sons, Ltd.

Look, D. C., Hemsky, J. W., & Sizelove, J. R. (1999). Residual native shallow donor in ZnO. *Physical Review Letters*, *82*, 2552–2555.

Madhuri, K. V. (2020). Thermal protection coatings of metal oxide powders. In *Metal Oxide Powder Technologies*, 209–231.

Makhlouf, A.S.H. (2011). Current and advanced coating technologies for industrial applications. In *Nanocoatings and Ultra-Thin Films*, 3–23.

Makhlouf, Abdel Salam Hamdy, & Rodriguez, R. (2019). Bioinspired smart coatings and engineering materials for industrial and biomedical applications. In *Advances in Smart Coatings and Thin Films for Future Industrial and Biomedical Engineering Applications*, 407–427.

Mao, Z., Shi, Q., Zhang, L., & Cao, H. (2009). The formation and UV-blocking property of needle-shaped ZnO nanorod on cotton fabric. *Thin Solid Films*, *517*, 2681–2686.

Mateen Tantray, A., & Shah, M. A. (2020). Photo electrochemical ability of dense and aligned ZnO nanowire arrays fabricated through electrochemical anodization. *Chemical Physics Letters*, *747*, 137346.

McLaughlin, R., & Glennon, J. D. (2011). Analytical methods: Spectroscopy, overview. In *Encyclopedia of Dairy Sciences: Second Edition*, 109–114.

Mika, K., Socha, R. P., Nyga, P., Wiercigroch, E., Małek, K., Jarosz, M., & Zaraska, L. (2019). Electrochemical synthesis and characterization of dark nanoporous zinc oxide films. *Electrochimica Acta*, *305*, 349–359.

Mtibe, A., Mokhothu, T. H., John, M. J., Mokhena, T. C., & Mochane, M. J. (2018). Fabrication and characterization of various engineered nanomaterials. In *Handbook of Nanomaterials for Industrial Applications*, 151–171.

Nair, G. B., & Dhoble, S. J. (2021). Phosphor-converted LEDs. In *The Fundamentals and Applications of Light-Emitting Diodes*, 87–126.

Naveed Ul Haq, A., Nadhman, A., Ullah, I., Mustafa, G., Yasinzai, M., & Khan, I. (2017). Synthesis approaches of zinc oxide nanoparticles: The dilemma of ecotoxicity. *Journal of Nanomaterials*, *2017*.

Neamen, D. A. (2003). The semiconductor in equilibrium. In *Semiconductor Physics and Devices*, *3*, 103–154.

Nicholson, J. W., & Parker, L. (1998). The chemistry of cements formed between zinc oxide and aqueous zinc chloride. *Journal of Materials Science*, *33*, 2251–2254.

Niederberger, M. (2007). Metal oxides: Chemistry and applications. Edited by J. L. G. Fierro. *ChemPhysChem*, *8*, 617–618.

Özgür, Ü., Alivov, Y. I., Liu, C., Teke, A., Reshchikov, M. A., Doğan, S., & Morkoç, H. (2005). A comprehensive review of ZnO materials and devices. *Journal of Applied Physics*, *98*, 041301.

Ozgur, Ü., Hofstetter, D., & Morkoç, H. (2010). ZnO devices and applications: A review of current status and future prospects. *Proceedings of the IEEE*, *98*, 1255–1268.

Patel, J. P., & Parsania, P. H. (2017). Characterization, testing, and reinforcing materials of biodegradable composites. In *Biodegradable and Biocompatible Polymer Composites: Processing, Properties and Applications*, 55–79.

Ponja, S. D., Sathasivam, S., Parkin, I. P., & Carmalt, C. J. (2020). Highly conductive and transparent gallium doped zinc oxide thin films via chemical vapor deposition. *Scientific Reports*, *10*, 1–7.

Porter, F., & International Lead Zinc Research Organization. (1991). *Zinc handbook: Properties, processing, and use in design.* New York: M. Dekker..

Pottathara, Y. B., Grohens, Y., Kokol, V., Kalarikkal, N., & Thomas, S. (2019). Synthesis and processing of emerging two-dimensional nanomaterials. In *Nanomaterials Synthesis: Design, Fabrication and Applications*, 1–25.

Ramírez-Amador, R., Alvarado, J., Flores-Carrasco, G., Morales-De la Garza, L., Alcántara-Iniesta, S., Luna-Flores, A., & Balcón-Camacho, J. (2020). The influence of deposition time on the structural, morphological, optical and electrical properties of ZnO-RgO nanocomposite thin films grown in a single step by USP. *Crystals*, *10*, 73.

Ramirez-Canon, A., Miles, D. O., Cameron, P. J., & Mattia, D. (2013). Zinc oxide nanostructured films produced via anodization: A rational design approach. *RSC Advances*, *3*, 25323–25330.

Raval, J. P., Joshi, P., & Chejara, D. R. (2018). Carbon nanotube for targeted drug delivery. In *Applications of Nanocomposite Materials in Drug Delivery*, 203–216.

Rimbu, C., Vrinceanu, N., Broasca, G., Farima, D., Ciocoiu, M., Campagne, C., & Nistor, A. (2013). Zinc oxide application in the textile industry: Surface tailoring and water barrier attributes as parameters with direct implication in comfort performance. *Textile Research Journal*, *83*, 2142–2151.

Schotten, C., Nicholls, T. P., Bourne, R. A., Kapur, N., Nguyen, B. N., & Willans, C. E. (2020,). Making electrochemistry easily accessible to the synthetic chemist. *Green Chemistry*, *22*, 3358–3375.

Shaikh, S. F., Ubaidullah, M., Mane, R. S., & Al-Enizi, A. M. (2020). Types, Synthesis methods and applications of ferrites. In *Spinel Ferrite Nanostructures for Energy Storage Devices*, 51–82.

Sharma, A. K. (2001). Semiconductor: An introduction. In *Semiconductor Electronics,* 1–14.

Singh, A. K. (2016). Experimental methodologies for the characterization of nanoparticles. In *Engineered Nanoparticles*, 125–170.

Souza, J. C. M., Bins-Ely, L., Sordi, M. B., Magini, R. S., Aparicio, C., Shokuhfar, T., & Cooper, L. (2018). Nanostructured surfaces of cranio-maxillofacial and dental implants. In *Nanostructured Biomaterials for Cranio-Maxillofacial and Oral Applications*, 13–40.

Suvaci, E., & Özel, E. (2020). Hydrothermal synthesis. In *Reference Module in Materials Science and Materials Engineering*, *2,* 73-80.

Wang, H., & Chu, P. K. (2013). Surface characterization of biomaterials. In *Characterization of Biomaterials*, 105–174.

Wang, Y., Chen, W., Wang, B., & Zheng, Y. (2014). Ultrathin ferroelectric films: Growth, characterization, physics and applications. *Materials*, *6*(9), 6377–6485.

Worsfold, P. J. (2004). Spectrophotometry - overview. In *Encyclopedia of Analytical Science: Second Edition*, 318–321.

Xia, Y., Wang, J., Chen, R., Zhou, D., & Xiang, L. (2016). A review on the fabrication of hierarchical zno nanostructures for photocatalysis application. *Crystals*, *6*, 148.

Yacobi, B. G. (2005). Basic properties of semiconductors. In *Semiconductor Materials*, 59–105.

Yadav, A., Prasad, V., Kathe, A. A., Raj, S., Yadav, D., Sundaramoorthy, C., & Vigneshwaran, N. (2006). Functional finishing in cotton fabrics using zinc oxide nanoparticles. *Bulletin of Materials Science*, *29*, 641–645.

Yan, J., Fan, Z., & Zhi, L. (2012). Functionalized carbon nanotubes and their enhanced polymers. In *Polymer Science: A Comprehensive Reference, 10*, 439–478.

Yan, Y. (2010). Tribology and tribo-corrosion testing and analysis of metallic biomaterials. In *Metals for Biomedical Devices*, 178–201.

Yao, C., Lu, J., & Webster, T. J. (2010). Titanium and cobalt-chromium alloys for hips and knees. In *Biomaterials for Artificial Organs*, 34–55.

Yavaş, A., Güler, S., & Erol, M. (2020). Growth of ZnO nanoflowers: effects of anodization time and substrate roughness on structural, morphological, and wetting properties. *Journal of the Australian Ceramic Society*, *56*(3), 995–1003

Yilmaz, E., & Soylak, M. (2019). Functionalized nanomaterials for sample preparation methods. In *Handbook of Nanomaterials in Analytical Chemistry: Modern Trends in Analysis*, 75–413.

Zhong, J., Chen, H., Saraf, G., Lu, Y., Choi, C. K., Song, J. J., & Shen, H. (2007). Integrated ZnO nanotips on GaN light emitting diodes for enhanced emission efficiency. *Applied Physics Letters*, *90*, 203515.